Applied Energy 336 (2023) 120801

Contents lists available at ScienceDirect

Applied Energy

journal homepage: www.elsevier.com/locate/apenergy

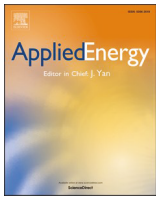

Probabilistic modeling of future electricity systems with high renewable energy penetration using machine learning

Martin János Mayer [a,*], Bence Biró [b], Botond Szücs [a], Attila Aszódi [b]

[a] Department of Energy Engineering, Faculty of Mechanical Engineering, Budapest University of Technology and Economics, Műegyetem rkp. 3, H-1111 Budapest, Hungary
[b] Institute of Nuclear Techniques, Faculty of Natural Sciences, Budapest University of Technology and Economics, Műegyetem rkp. 9, H-1111 Budapest, Hungary

HIGHLIGHTS

- Easy-to-use machine learning model for hourly renewable production and load profile modeling.
- Novel variance-correction method to improve the reliability of the modeled profiles.
- Probabilistic energy supply simulation based on 42 years of meteorological data.
- Detailed evaluation and novel categorization of Dunkelflaute events.
- Uncertainty analysis of the share of photovoltaic, wind and nuclear electricity.

GRAPHICAL ABSTRACT

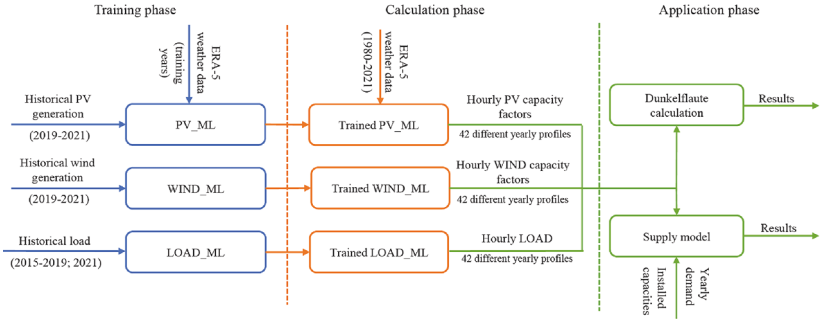

ARTICLE INFO

Keywords:
Probabilistic simulation
Neural network
Hourly profile
Dunkelflaute
Security of supply
Carbon-free electricity generation

ABSTRACT

The increasing penetration of weather-dependent renewable energy generation calls for high-resolution modeling of the possible future energy mixes to support the energy strategy and policy decisions. Simulations relying on the data of only a few years, however, are not only unreliable but also unable to quantify the uncertainty resulting from the year-to-year variability of the weather conditions. This paper presents a new method based on artificial neural networks that map the relationship between the weather data from atmospheric reanalysis and the photovoltaic and wind power generation and the electric load. The regression models are trained based on the data of the last 3 to 6 years, and then they are used to generate synthetic hourly renewable power production and load profiles for 42 years as an ensemble representation of possible outcomes in the future. The modeled profiles are post-processed by a novel variance-correction method that ensures the statistical similarity of the modeled and real data and thus the reliability of the simulation based on these profiles.

The probabilistic modeling enabled by the proposed approach is demonstrated in two practical applications for the Hungarian electricity system. First, the so-called Dunkelflaute (dark doldrum) events, are analyzed and categorized. The results reveal that Dunkelflaute events most frequently happen on summer nights, and their typical duration is less than 12 h, even though events ranging through multiple days are also possible. Second, the renewable energy supply is modeled for different photovoltaic and wind turbine installed capacities. Based on our calculations, the share of the annual power consumption that weather-dependent renewable generation

* Corresponding author.
E-mail address: mayer@energia.bme.hu (M.J. Mayer).

https://doi.org/10.1016/j.apenergy.2023.120801
Received 2 August 2022; Received in revised form 6 January 2023; Accepted 3 February 2023

can directly cover is up to 60% in Hungary, even with very high installed capacities and overproduction, and higher carbon-free electricity share targets can only be achieved with an energy mix containing nuclear power and renewable sources. The proposed method can easily be extended to other countries and used in more detailed electricity market simulations in the future.

Nomenclature

Abbreviations

AMeDAS	Automated Meteorological Data Acquisition System
ANN	Artificial Neural Networks
CBT	Constantly Below Threshold
CPU	central processing unit
DL	deep learning
ECMWF	European Centre for Medium-Range Forecasts
ERA5	ECMWF reanalysis version 5
GBM	gradient boosting
GHI	global horizontal irradiance
GSA	Global Sensitive Analysis
LMP	Local Marginal Price
LPD	load probability distribution
LSTM	Long Short Term Memory
LWP	low-wind-power
MAE	mean absolute error
MAPE	mean absolute percentage error
MBT	Mean Below Threshold
MPE	mean percentage error
MRPE	maximal relative percentage error
MSE	mean squared error
PICP	prediction interval coverage probability
PINAW	prediction interval normalized average width
PSO	Particle Swarm Optimization
PV	photovoltaic
RF	random forest
RMSD	root-mean-square deviation
RMSE	root mean squared error
RNN	Recurrent Neural Network
SCC	squared correlation coefficient
SD	standard deviation
SVM	Support Vector Machines
SVR	Support Vector Regression
VRE	variable renewable energy
WP	weather pattern

1. Introduction

The number and capacity of weather-dependent renewable energy production units have exploded in recent years [1]. Increasing the share of renewables is included in most energy policy objectives. However, in many European countries, conventional power plant units are being decommissioned, partly due to decarbonization targets. The increasing share of renewable energy sources (RES) and the decreasing share of conventional power plants raises questions on system stability and security of energy supply. If the current trend continues, the reliability of the power production and consumption forecasts will determine the reliability of electricity systems. As we seek to rely more and more on renewables, the phenomenon of “Dunkelflaute” (hereafter abbreviated as DF, known as “dark doldrum” in the English-speaking and “anticyclonic gloom” in the meteorological world [2]), where load factors of wind and solar photovoltaic (PV) generation units are negligible, is becoming increasingly critical for countries conducting energy transition [2–4]. On the other hand, the security of energy supply is critical not only from a technical point of view, but also for the sustainability of the energy transition. In order to keep the support of the society for this development, such technical solutions are required that can ensure a continuous and reliable electricity supply. There are several studies that examined energy mix modeling [5,6] and optimization of energy resource mix [7–11]. The probabilistic forecasting of renewable energy production has also been the subject of many studies [12–16].

By analyzing of National Energy and Climate Plans of European countries, it was observed that in such high-level documents, governments tend to oversimplify the calculations used as the basis for the analysis of different energy scenarios [17]. However, it was proven in several studies [7,10] that at least hourly resolution modeling of the future energy mixes is required to determine which proportion of the total demand the weather-dependent renewable technologies can supply and how big capacity of flexible power plants will be required to keep the system operational. Sharifzadeh et al. [18] predicted wind and PV production to minimize the need for electricity storage and standby capacities. Livas-Garícia et al. [19] have developed a market model that can be used to investigate the market potential of regulating power plants. Modeling the future energy mix at an hourly resolution not only helps to better integrate renewable capacities, but also shows the market potential of balancing capacities. Further use of such a model is to investigate different energy storage systems (daily, weekly and seasonal) and to determine the optimal storage mix.

It is a common practice to scale and project the annual production/load profile from recent years to the future, but it does not take into account the variability of weather, which undermines the reliability of this practice [20,21]. Solar and wind energy productions are estimated from probability distribution functions in several papers, e.g., Arriagada et al. [22] applied bimodal normal distribution for PV and wind production, Rakipour et al. [23] used Weibull distribution for wind speed prediction and probability distribution functions (PDF) for solar irradiance, and Ling Li et al. [24] used Rayleigh probability distribution function for wind speed prediction and Beta distribution function for solar prediction. However, these distributions are not related to the actual weather, so this is not a reliable way to model PV and wind energy production in the long term, as weather variability can only be taken into account by looking at longer time series. A summary of the papers dealing with high-resolution modeling of renewable generation and load profiles is shown in Appendix C, Table C.9. Key aspects of this summary are the time step and domain, the methodology, the databases used, and the evaluation and utilization of the resulting profiles. Still, only a few of these studies offer a possibility to quantify the uncertainty resulting from the year-to-year variability of the weather conditions.

Uncertainty can be quantified by an ensemble method, where not only one year’s data is used, but several decades from the past, as long we can believe that the weather in the future will be somewhat similar to the past. The fluctuating availability of renewable energy sources has also been a known problem in the context of hydropower for several decades. Many electricity systems with a high share of hydropower face resource shortages when river levels fall. Such electricity systems are found in some countries in South America [25–27] and Europe, typically in the Balkans [28]. However, while hydropower production can be

predicted for weeks or months by monitoring rainfall in water catchment areas, the forecasting of wind and PV power production is much more complicated, and the dynamic of production change is faster.

As discussed above the detailed analysis of future electricity systems with a high share of weather-dependent RES requires hourly generation and load profiles covering many years. However, weather dependent RES data are in many countries only available for several years due to the fact that most countries have started to build high renewable generation capacities in the last five to ten years. In contrast, atmospheric reanalyses made historical hourly weather data covering multiple decades available worldwide, which offers a good source to assess the natural variability of RES. Wohland et al. [29] went even further, and found, based on a reanalysis of 110 years of wind speed data, that even multidecadal wind variability over such time scales have a significant impact on wind power generation. In order to make use of these long-term weather data in energy system simulations, a novel method based on machine learning is proposed here that maps the weather data to renewable power generation and electric load. Baumgartner et al. [30] have also used neural networks to reproduce the production of wind power plants in Germany using the MERRA-2 database. This approach makes it possible to create synthetic hourly generation and load profiles for multiple decades in which weather data are available, which is suitable for probabilistic simulations by treating the profiles from multiple years as an ensemble. The advantage of this methodology compared to physical models [31,32] is that there is no need to collect labor-intensive data (e.g. spatial distribution of installed capacity), but only publicly available data is sufficient to obtain the appropriate result.

This method can be applied to any country that has historical renewable generation and electric load data covering at least two or three years; however, without the loss of generality, it is presented in this paper for the case of Hungary. The electricity supply of Hungary currently relies heavily on nuclear energy, fossil fuels and imports [17]. The country's annual electricity consumption in 2021 was 47 TWh,[1] with a peak system load of 7 361 MW.[2] In the Hungarian electricity system, besides further sources that are not in the scope of the present analysis, there were 1830 MW solar PV, 320 MW wind, and 2000 MW nuclear installed capacities.[3] The future of the country's energy sector is set out in two government documents: the National Energy and Climate Plan [33] and the National Clean Development Strategy 2020–2050 [34]. These documents forecast a significant increase in electricity consumption in the country (58 TWh in 2030, 67 TWh in 2040, and up to 83 TWh in 2050 due to widespread electrification) and a shift in the electricity generation from fossil to solar (in the Hungarian system the solar PV capacity could be 6 GW in 2030, 12 GW in 2040 and up to 60 GW in 2050), while maintaining the current presence of nuclear power and a moderated level of imports.

The main contribution of this paper is to present an easy-to-use yet effective machine learning (ML) method for the probabilistic modeling of the future load and weather-dependent renewable generation profiles simultaneously. This method can be applied to any country worldwide where at least a few years of historical generation and load datasets are available. An essential part of this procedure is a novel variance-correction method that ensures the statistical similarity of the modeled and real profiles. Based on 42 years of historical weather data, probabilistic estimations were made on how inter-annual weather variability affects renewable electricity generation. Quantifying the weather-related uncertainties can help to make better decisions related to the energy strategy.

The proposed method is demonstrated in two practical applications, which are the modeling of Dunkelflaute events and the future electricity mix in Hungary. These parts also show how the uncertainty quantified by probabilistic modeling can be visualized in different kinds of diagrams. A novel categorization method is also proposed, which classifies the severity of Dunfelklaute events based on the load of the electricity grid.

The weather, load and generation data and the proposed methodology, including the machine learning, variance correction, and the Dunkelflaute and energy mix modeling, are presented in Section 2. The detailed process and the validation of the ML-based synthetic PV, wind, and load profile generation are described in Section 3. Two possible applications of the proposed method, namely the probabilistic modeling of the Dunkelflaute events and future energy mix, are discussed in Section 4. The main conclusions are drawn in Section 5.

2. Data and methods

The reliable probabilistic modeling of renewable energy production in the future requires as many years of historical data as possible to cover the possible widest range of weather conditions. Historical renewable power generation data are only available from the last several years in most countries; however, historical meteorological data have been collected for decades. Based on this, the overarching idea of the proposed method is as follows: first, the relationship between the meteorological data and the country-wide PV and wind power generation and system load is mapped by machine learning models. In the next step, the trained models are used to generate power generation and load profiles synthetically for multiple decades based on the long historical meteorological datasets, which is 42 years in this case. Finally, the yearly profiles of 42 years enable to perform the energy mix simulation separately with the data for each year, resulting in 42 different outcomes, which can be used then as an ensemble, allowing to assign uncertainty information for all results.

This section presents the meteorological (Section 2.1) and the Hungarian solar and wind power production and electric load data (Section 2.2), the proposed artificial neural network (Section 2.3), the variance-correction of the modeled data (Section 2.4), and the calculations behind the applications presented in Section 4 of the paper (Section 2.5).

2.1. Weather data

The first step of the presented probabilistic energy mix modeling methodology is to obtain historical weather data covering as much as possible from the previous decades. The most important meteorological variables for this purpose are ambient temperature, solar irradiance, and wind speed. The most accurate weather data source is ground-based measurement; however, its usage has several practical limitations, including limited spatial coverage, restricted availability, and possible inconsistencies over time. To circumvent these drawbacks, most researchers rely on gridded weather datasets created by atmospheric reanalysis. The aim of the reanalysis is to produce a complete and consistent historical weather dataset by applying the data assimilation system and physical models used for numerical weather predictions on historical observations. The two most well-known global reanalysis products are the 5th version of the European Centre for Medium-Range Weather Forecasts (ECMWF) Reanalysis (ERA5) [35] and the Modern-Era Retrospective analysis for Research and Applications, Version 2 (MERRA-2) [36]. Both reanalyses offer hourly data for more than four decades with global coverage, but ERA5 has a higher, 0.25° spatial resolution compared to the 0.5° of the MERRA-2. Moreover, a recent validation of the global horizontal irradiance (GHI) of the two datasets revealed higher accuracy for the ERA5 [37]; therefore, that reanalysis is used and recommended in this study as a source of meteorological data.

The ERA5 data can be retrieved from the Climate Data Store (CDS) of the Copernicus Programme. The weather data required for the purpose of this study can be found in the "hourly data on single levels" dataset

[1] https://www.mavir.hu/documents/10258/240293410/R%C3%A9szletes+havi+brutt%C3%B3+energia+adatok+2021_12+HU+.pdf.
[2] https://mvm.hu/hu-HU/Tevekenysegunk/AtvitelRendszerIranyitas.
[3] https://www.mavir.hu/documents/10258/240839410/BT_2015-20220701_ig_BR+NT_HU.pdf.

Table 1
Annual average capacity factor of PV and wind power plants in Hungary between 2019 and 2021[a].

	2019	2020	2021
PV	16.01%	16.35%	16.87%
Wind	23.02%	21.00%	21.80%

[a]https://www.mavir.hu/documents/10258/240748006/PV + STATISZTIKA_-HU_20220601_ig_v2.pdf.

Table 2
Minimum, average, and maximum electric load and annual electricity consumption of Hungary in the years 2015–2021.

	2015	2016	2017	2018	2019	2020	2021
Minimum system load, MW	3 152	3 237	3 332	3 210	3 394	3 167	3 525
Average system load, MW	5 001	5 023	5 151	5 193	5 215	5 134	5 340
Maximum system load, MW	6 424	6 707	6 746	6 805	7 072	7 058	7 332
Total annual consumption, TWh	43.8	44.1	45.1	45.5	45.7	45.1	46.8

under the following names:

- Surface solar radiation downwards,
- 2 m temperature,
- 10 m u-component of wind,
- 10 m v-component of wind,
- 100 m u-component of wind,
- 100 m v-component of wind.

The data requests can be submitted through both an interactive website[4] and the CDS Application Program Interface (API)[5] in Python language. The interactive website also provides the code for the API request matching the selected data configuration. Therefore, the easiest way to obtain data for multiple years is to configure the request for one year in the interactive surface, copy the resulting API code to a Python script, and automatically download the data for all years in separate files using a simple loop. The meteorological data used in this paper was downloaded for the 42 complete years from 1980 to 2021 with an hourly resolution for Hungary.

The geographical area of the data is set to the smallest sub-region that covers the whole country. However, even after this spatial subsetting, some of the downloaded grid points fall outside the borders of the country, and the weather in those points is not expected to affect the renewable energy production inside the country. These unnecessary grid points are filtered based on the Nominatim[6] reverse geocoding web service of OpenStreetMap, which returns the address for the requested geographical coordinates: if the country field of the address is Hungary, the grid point is kept, otherwise it is deleted. If necessary, the address provided by the reverse geocoding could also be used for grouping the data, e.g., by states or counties. The number of grid points in Hungary is 177.

The unit of the surface solar radiation downwards variable is J/m^2, which has to be divided by 3600 s, the length of the accumulation period, to convert it to the hourly average global horizontal irradiance in W/m^2. The 2 m temperature and the wind speed are in °C and m/s, thus, no further unit conversion is required. The v is the northward, while the u is the eastward component of the wind speed, while the absolute wind speed can be calculated as the norm of the vector using the Pythagorean theorem.

2.2. Electric load and renewable power generation data

In addition to the data describing the weather, we needed information about the Hungarian solar PV and wind power plants and the Hungarian electricity consumption (system load) to perform the calculations. These were hourly production data and installed capacities for solar PV and wind power plants and hourly system load data for electricity consumption. These data were downloaded from the website[7] of the Hungarian Transmission System Operator (TSO), MAVIR Zrt. The quality of these datasets is good, with no missing or spurious (e.g., negative) entries. For other countries, the above data may be available from the websites of the TSOs of the countries concerned or, for European countries, from the ENTSO-E Transparency Platform.[8] However, in the case of the ENTSO-E data source, a higher emphasis should be placed on data quality control due to the shortcomings described in [17].

The hourly power generation data of the PV and wind power plants are downloaded for the three years of 2019–2021. To normalize these data and remove their increasing trend, the power outputs are converted to capacity factors by dividing them by the actual installed capacity. The installed capacity data is also available from the TSO; however, only with a monthly resolution, which must be downscaled to an hourly resolution to match the power generation data. The downscaling is performed by linear interpolation between the known data points, as this method ensures the best accuracy. The effect of the original resolution of the installed capacity data and the different downscaling methods are assessed in Appendix A.

The hourly resolution system load values are downloaded for the period 2015 to 2021, and as a pre-processing before using them to train the ML models, they are normalized to the average for the given year. Data for 2020 are not used for the training of the model as it is highly affected by the negative impacts of COVID-19 pandemic on Hungary's electricity consumption [38], so using the unrepresentative data of this year would have led to less accurate results.

The average capacity factors of PV and wind power plants and electricity consumption in Hungary are presented in Table 1 and 2.

2.3. Neural network

The relationship between the meteorological variables and renewable power production or electricity demand can be modeled using, among others, nonlinear regression. Machine learning enables the regression to be performed without any prior assumptions about the shape of the function between the predictors (inputs) and the predictand (output). Many different ML models exist that can perform nonlinear regression. The current machine learning libraries in popular programming languages, like *scikit-learn* in Python and *caret* in R, include a wide range of models with a common, easy-to-use interface and thus enable the practical use of ML without a deeper interaction with the underlying mathematics. The most popular and versatile ML model is the artificial neural network (ANN), which was inspired by the working principle of biological neural systems. ANN shows a good performance in a wide range of tasks, including the mapping of weather data to solar PV power production, as shown in a comparison of 24 ML models for operational PV power forecasting [39].

The basic unit of an ANN is an artificial neuron, which has multiple inputs and one output, and the output is calculated by applying a nonlinear activation function on the weighted sum of the input signals

[4] https://cds.climate.copernicus.eu/cdsapp#!/dataset/reanalysis-era5-single-levels?tab=form.

[5] The CDS API client is the *cdsapi* Python package, see further details: https://cds.climate.copernicus.eu/api-how-to.

[6] https://nominatim.org/.

[7] https://www.mavir.hu/web/mavir.

[8] https://transparency.entsoe.eu.

Table 3
Summary of the tuned hyperparameters of the neural network.

Hyperparameter		Tested values
Number of neurons	One hidden layer	10
		50
		100
		200
	Two hidden layers	10, 10
		20, 20
		50, 50
Learning rate		0.001
		0.01
		0.1
Activation function		$\mathrm{ReLU}(x) = \max(0, x)$
		$\tanh(x) = \frac{e^{x} - e^{-x}}{e^{x} + e^{-x}}$
		$\mathrm{sigmoid}, \sigma(x) = \frac{1}{1 + e^{-x}}$

[40]. Typical activation functions are the sigmoid logistic function, the hyperbolic tangent, and the rectified linear unit (ReLU). The neurons can be organized into a wide range of different architectures, of which the advanced ones belong to the family of deep learning models. In this study, a simple multilayer perceptron (MLP) is used, where the neurons are arranged into subsequent layers. The input layer has one neuron for each predictor, which does not process the data but only passes them forward to the following layer. This is followed by one or multiple hidden layers, each having an arbitrary number of neurons, while the last layer is the output layer with one neuron with a linear activation function for each predictand [41].

The parameters of the MLP are the weights of the neurons, and the aim of the training is to find the parameters that ensure the best mapping between the predictors and the predictand of the model. The optimal parameters are typically found by a stochastic gradient-based optimization method, where the objective of the optimization is to minimize a loss function that represents the errors of the modeled output. The gradients of the loss function with respect to the parameters are derived by the backpropagation algorithm, and the change of each parameter in an iteration step is proportional to the gradient and a learning rate.

Machine learning models also have hyperparameters, which are set in advance of the training, and affect both the convergence of the training and the final performance of the model. In a MLP, the most important hyperparameters are the number of neurons and hidden layers, the activation function, and the learning rate [42]. To ensure the best accuracy, the hyperparameters are selected by a tuning process, in which different hyperparameter combinations are tested using a grid search algorithm with a K-fold cross-validation, where K is selected as the number of the years. i.e., one year is used for testing and the others for training in each iteration step. The hyperparameters resulting in the lowest errors on the test data are used for the final estimations. The tested values of the three tuned hyperparameters are listed in Table 3. The overfitting of the model is avoided by an early stopping routine. 10% of the training data is set aside for validation, and the training stops if the score on the validation set does not show at least 10^{-4} relative improvement over 10 consecutive epochs.

In this paper, the MLP is implemented by the *MLPRegressor* class of the *scikit-learn* Python package. Three different MLP models are created and trained, one for the PV capacity factor modeling, named PV_ML, another for the wind capacity factor modeling under the name WIND_ML, and the third for the mean-normalized electric load modeling, called LOAD_ML. The details of these three models, including the predictors, the tuned hyperparameters, and the achieved accuracy, are presented in Sections 3.1–3.3 seperately for the three models.

2.4. Variance-correction of modeled data

All regression models require a loss function that is minimized during the training of the model. The most commonly used loss function is the mean square error (MSE), which weights all errors proportional to the size of the error, i.e., penalizes higher errors disproportionally more than lower ones. That said, in a wide range of applications, including the modeling of renewable energy production and load profiles, the most important is to ensure the statistical similarity between the measured and estimated data, which can be best reflected by similar probability density functions (PDF). A necessary condition of similar PDFs is to have the mean and the variance of the measured and estimated datasets as close as possible, respectively. However, as highlighted in a recent paper in the context of solar forecasting [43], MSE-optimized estimates are always underdispersed. The underdispersion means that the estimated data has a lower variance than the measured data, and the extremely low and high values are less frequent in the modeled data than in reality, which can fundamentally undermine the reliability of all studies that use modeled data for analyzing extreme events.

The inevitable underdispersion is plain to see from the well-known bias-variance decomposition of the MSE,

$$\mathrm{MSE}(f,x) = \mathbb{V}(f) + \mathbb{V}(x) - 2\rho(f,x)\sqrt{\mathbb{V}(f)\mathbb{V}(x)} + \mathrm{MBE}^2(f,x) \tag{1}$$

where f and x are the modeled (forecast) and measured data, respectively, $\mathbb{V}(.)$ is the variance, ρ is the correlation coefficient, and MBE is the mean bias error. Eq. (1) can be rearranged into the format

$$\mathrm{MSE}(f,x) = \left[1 - \rho^2(f,x)\right]\mathbb{V}(x) + \left[\sigma(f) - \rho(f,x)\sigma(x)\right]^2 + \mathrm{MBE}^2(f,x) \tag{2}$$

where $\sigma(.) \equiv \sqrt{\mathbb{V}(.)}$ is the standard deviation. From Eq. (2), it follows that the MSE is minimized only if $\mathrm{MBE}(f,x) = 0$, and $\sigma(f) = \rho(f,x)\sigma(x)$. Insofar as the $\rho(f,x)$ correlation coefficient is lower than 1, which always holds for a model with inaccuracy, the variance of the modeled data is lower than that of the measured. The lower the correlation coefficient is, the more underdispersed the estimates are.

The simplest way to correct the variance of the estimations is a linear calibration,

$$f' = af + b \tag{3}$$

where a and b are the scale and offset parameters, respectively. In order to correct the variance of the modeled data, the scale parameter should be set to the ratio of the standard deviations of the observations and the estimates, which is, for an MSE-optimized model, theoretically equal to the reciprocal of the correlation coefficient,

$$a = \sigma(x)/\sigma(f) = 1/\rho(f,x) \tag{4}$$

Scaling the estimates also changes the bias, which can be remedied by selecting the offset parameter as

$$b = \mathbb{E}(x) - a\mathbb{E}(f) \tag{5}$$

The scale and offset parameters can be derived using the correlation coefficient and the mean of the observations and estimates calculated for the training data, and then the linear correction can be used to post-process the raw estimates for any unknown datasets. A more detailed description of this method can be found in [43]. The effect of the linear variance correction is demonstrated for the wind power factor estimation in Appendix A.

2.5. Dunkelflaute and electricity supply modeling

The hourly-resolution data series of weather-dependent renewable energy production and system load generated by the method presented in this paper can be used in several practical applications, two of which are discussed in more detail in this paper: modeling the primary energy composition of the electricity production, and investigating Dunkelflaute conditions in which both solar PV and wind productions are low or even negligible.

A DF event is a condition in which solar, onshore wind and offshore wind all have low capacity factors. Hungary is landlocked, thus it has no

possibility for offshore wind turbines, so in this paper, an hour is considered to be in DF state if the capacity factors of solar and onshore wind in Hungary are both below a given threshold value. Several different examples of the DF threshold can be found in the literature, e.g., [2,4,44] define it as 10%, and [3] uses 2%, 5% and 10% thresholds. As there is no consensus about a standardized DF threshold value, three different thresholds of 1%, 5%, and 10% are used in this paper. Mathematically, DF is described as follows:

$$DF^i = \left(CF^i_{PV} < TH\right) \wedge \left(CF^i_{wind,on} < TH\right) \tag{6}$$

where DF is a Boolean indicating whether the i th hour is Dunkelflaute or not, CF^i_{PV} and $CF^i_{wind,on}$ are the PV and the onshore wind capacity factors in the i th hour, respectively, and TH is the threshold below which a DF event is interpreted. In countries with potential offshore wind power plants, a term with $CF_{wind,off} < TH$ should also be added to Eq. (6) to account for the offshore wind power plants.

The future energy mix is modeled with a simplified hourly resolution electricity supply model of Hungary in 2030, which only includes the electric load on the consumer side and the solar, wind, and nuclear capacity on the generation side (these capacities are at the beginning of the merit order due to their low variable costs [45,46]). As the main aim of this simple model is to identify the possible share of renewable and carbon-free generation in supplying the electricity consumption, there is no need to model further conventional power plants. Hydropower is not considered for two reasons, 1) modeling of hourly resolution hydropower generation is not the scope of this research, and 2) hydropower is not currently dominant in Hungary, nor do government documents anticipate its growing role.

The hourly resolution electric load data are obtained by multiplying the normalized load data, estimated by the LOAD_ML model, by the average annual electric load. The average load can be calculated from the expected total annual energy consumption by dividing it by the length of the years. In the year 2030, the annual electricity consumption of Hungary is projected to be 57.839 TWh [33], which equals an average 6602.6 MW system load.

The hourly resolution PV and wind power generation time series are the product of the capacity factors estimated by the PV_ML and WIND_ML models and the respective projected PV and wind installed capacity, which are assumed to be constant during the modelled year.

$$P^i_{gen,RES} = CF^i_{PV} IC_{PV} + CF^i_{wind,on} IC_{wind,on} \tag{7}$$

where $P^i_{gen,RES}$ is the renewable power generation in the i th hour, and IC_{PV} and $IC_{wind,on}$ are the installed capacities of the PV plants and wind turbines, respectively.

The assumed nuclear power plant is the Paks power plant in Hungary, which has four units with 500 MW installed capacity each. In our model this is defined as a base load power plant in the Hungarian electricity system, i.e., it is assumed to generate 2000 MW power every hour of the year, except from May to August. In these months, one of the units is assumed to be under maintenance and refueling, resulting in a constant 1500 MW output by the remaining three units. The carbon-free power generation is calculated as the sum of renewable and nuclear power, and it is calculated as:

$$P^i_{gen,CF} = CF^i_{PV} IC_{PV} + CF^i_{wind,on} IC_{wind,on} + P^i_{nuc} \tag{8}$$

where $P^i_{gen,CF}$ is the carbon-free and P^i_{nuc} is the nuclear power generation in the i th hour.

Given the yearly generation and load time series, the next step is to calculate what part of the load can be covered by the renewable generation in each hour. The load served by renewable generation can be calculated as:

$$P^i_{served} = \min\left(P^i_{gen,RES}, P^i_{load}\right) \tag{9}$$

where P^i_{served} is the load served by the renewables, and P^i_{load} is the total system load in the i th hour. This served power can also be called useful power, as this is the part of the renewable power generation that can directly be used by the consumers. If the renewable generation is higher than the load, the excess generation is considered overproduction, calculated as:

$$P^i_{over} = \max\left(0, P^i_{gen,RES} - P^i_{load}\right) \tag{10}$$

The hourly served (useful) and excess energy is calculated by summing the hourly power values over the year multiplied by the length of the timestep:

$$E = \sum_{i=1}^{8760} P^i \Delta t \tag{12}$$

where E is the annual energy, and $\Delta t = 1\text{h}$ is the length of a timestep.

The share of the annual consumption covered by renewable energy sources is calculated as:

$$S_{RES} = \frac{E_{served}}{E_{load}} = \frac{\sum_i P^i_{served}}{\sum_i P^i_{load}} \tag{13}$$

where S_{RES} is the share of direct renewable production in the total consumption.

All calculations in Eq. (9–13) can also be performed for carbon-free generation, which also includes nuclear power, instead of only renewables by simply substituting $P^i_{gen,RES}$ to $P^i_{gen,CF}$ in all equations.

All the above-presented calculations rely on the time series data for one year. Using the ML models, hourly-resolution profiles are generated for all 42 years, which enables to perform all the above-presented calculations independently for each year, yielding 42 slightly different results. These 42 outcomes are then treated as members of an ensemble, each having an equal probability of representing the expected weather conditions in 2030, and the spread of the outcomes indicates the uncertainties resulting from the weather variability. Mathematically, the results calculated for the 42 different sets of profiles are sorted into ascending order and converted into a probability density function assuming uniform spacing between each member.

3. Modeling renewable power generation and electricity demand profiles

The detailed description of the machine learning model used for the renewable energy generation (PV_ML and WIND_ML model) and electricity demand profile calculation (LOAD_ML model) and the evaluation of the accuracy of the estimated profiles are summarized in the following subsections. The predictors were selected in an iterative process, and only the final set is presented in all three cases. The historical data used for the training and testing of PV_ML and WIND_ML models cover the three years of 2019–2021 for the PV and wind power, and the six years of 2015–2021 for the electricity demand modeling in LOAD_ML model (excluding 2020 due to the unrepresentative effects of the COVID-19 pandemic [38]). The evaluation of the modeled data is performed using K-fold cross-validation, in which the full historical dataset is divided into yearly subsets (i.e., K equals the number of years). For each year, the training is performed using the data only from the other years, and the evaluation is performed for the year of interest. In this way, it is possible to evaluate how the model performs on unseen data.

The best convergence of MLP requires having all input and output data scaled to the same order of magnitude. All predictors of the MLP are scaled into the range of 0 to 1 by a linear transformation in order to improve the convergence of the training. From the predictands, the PV and wind capacity factors are naturally bounded by 0 and 1; therefore, no further scaling is required. The electric load is already normalized by its yearly average value during the pre-processing, squeezing the data into a range of 0.65–1.35, which is also suitable for the MLP without

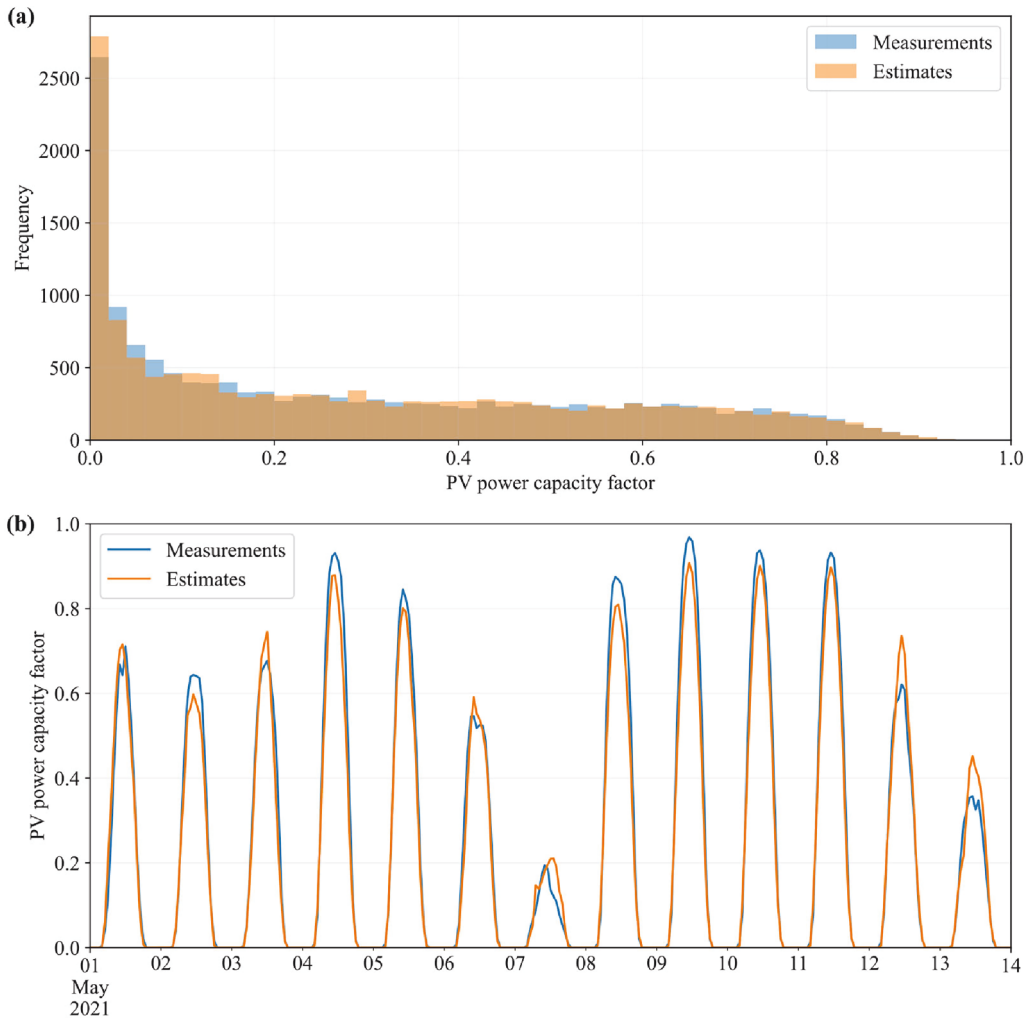

Fig. 1. Daytime hourly national PV capacity factor observations and estimates, (a) histogram for the three years of 2019–2021, (b) time series plot for a randomly selected sample period of 1st to 14th May 2021.

further scaling.

The accuracy of the estimated data is evaluated using the five metrics. The correlation coefficient reflects the potential accuracy of the modeled data regardless of its calibration [47], and it is calculated as

$$\rho = \frac{\mathrm{cov}(f,x)}{\sigma(f)\sigma(x)} \tag{16}$$

where f and x are the modeled (forecast) and measured data, respectively, and $\mathrm{cov}(.)$ is the covariance. The mean bias error (MBE) is the average of all errors, and large positive or negative values indicate a systemic overestimation or underestimation, respectively.

$$MBE = \frac{1}{N}\sum_{i=1}^{N}(f_i - x_i) \tag{17}$$

where N is the number of samples. The mean absolute error (MAE) is the average of the absolute value of all errors, and it is equally sensitive to the small and large errors regardless of their direction.

$$MAE = \frac{1}{N}\sum_{i=1}^{N}|f_i - x_i| \tag{18}$$

The root mean square error (RMSE) penalizes the higher errors more, making it the most sensitive to the outliers.

$$RMSE = \sqrt{\frac{1}{N}\sum_{i=1}^{N}(f_i - x_i)^2} \tag{19}$$

Finally, the variance ratio, which is introduced in [48] as the ratio of the variance of the estimated and measured data, gives a one-number summary of the dispersion of the estimations. A variance ratio higher or lower than one indicates overdispersed or underdispersed forecasts, respectively.

$$F = \frac{\mathbb{V}(f)}{\mathbb{V}(x)} \tag{20}$$

In addition to these metrics, three graphs are also presented in each case to provide a complete picture of the reliability of the estimations (see the first examples in Fig. 1 (a), Fig. 1 (b) and Fig. 2):

- a histogram visualizing the distribution of the measured and modeled data,
- a time series plot of the measured and modeled profiles for a sample period, and
- an error "heat map" showing the differences between the modeled and real data for all 8760 h of the year in a matrix form (hours per day on the y-axis, days of the year on the x-axis), values represented by colors.

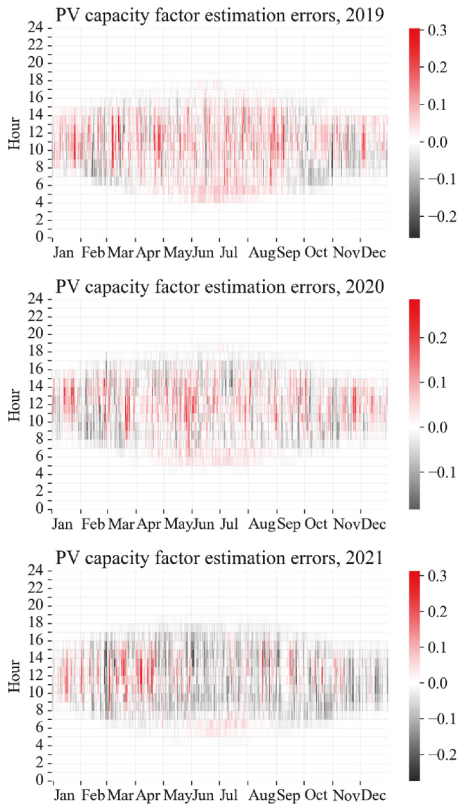

Fig. 2. Time-dependence of the hourly PV power capacity factor errors.

Table 4
Error metrics of the national PV power capacity factor estimations in PV_ML model. All metrics are calculated for the cross-validation steps when the given year is used as the test data.

	2019	2020	2021	Overall
Correlation coefficient	0.986	0.987	0.985	0.985
MBE	0.006	0.001	−0.009	−0.001
MAE	0.020	0.019	0.023	0.021
RMSE	0.041	0.039	0.045	0.042
Variance ratio	105.4%	100.0%	91.4%	98.7%

3.1. Photovoltaic power capacity factor modeling (PV_ML model)

Theoretically, the power output of a PV system depends on the global irradiance on the module surface and the cell temperature. The irradiance on a tilted plane can be estimated from the horizontal irradiance by a transposition model [49]. Transposition models treat the beam and diffuse irradiance differently; therefore, the GHI must be decomposed first into these two components using a separation model. In this paper, the Engerer [50] separation and Perez [51] transposition models are used to calculate the global tilted irradiance (GTI) due to their good performance in previous studies [49,52]. The separation and transposition modeling also requires the position of the Sun, which is calculated using the Solar Position Algorithm (SPA) [53] based on the date and time and the geographic coordinates. Even though ML could be capable of learning the irradiance transposition without physical modeling, the pre-calculation of GTI improves the accuracy of the PV power estimation. In this particular case, adding GTI to the inputs improved the overall correlation from 0.983 to 0.985. A recent paper has also shown that the GTI is an important and more effective predictor than either the hour of the day or the Sun position angles for the ML-based estimation of PV production [42].

The orientation of the PV modules may be very different in the distinct PV plants, and it is not known in detail; therefore, the GTI is calculated for a representative, quasi-optimal orientation. The plane of maximum irradiation in Hungary has a 35° tilt angle and south-facing azimuth; however, it is common for PV plants to use a lower tilt angle to avoid excessive shading and reduce the costs of the mounting structure [54]. Based on these assumptions, the GTI is calculated for a south-facing surface with a 30° tilt angle at all grid points. The GHI and GTI are both included among the predictors, as based on their difference, the MLP may also be able to estimate the irradiance on differently oriented module planes.

The cell temperature is affected by the ambient temperature, the GTI, and the wind speed. The effect of wind speed on the PV power is typically low. If the wind speed data is not measured but modeled or forecasted, and therefore it has a significant inaccuracy, then considering it in the model may also decrease the accuracy of the calculated PV power [48]. For this reason, wind speed is not included in the PV power estimation as a predictor. The cell temperature affects the PV output only moderately through the module efficiency; therefore, the ambient temperature data are not used individually for all grid points, but their average is calculated for the whole grid, and it is included as a single predictor.

The timesteps with zero GHI in all grid points are identified as nighttime and filtered out from the training data of the PV_ML model. Similarly, during the generation of the modeled PV profiles, the trained PV_ML model is only used to estimate the solar PV load factor for the daytime periods, while night values are automatically set to zero.

The predictand of the network is the aggregated national PV capacity factor. The predictors were selected based on iterative testing of several different input scenarios. The recommended set of predictors of the MLP are (355 inputs in total):

- global horizontal irradiance individually for all grid points,
- global tilted irradiance individually for all grid points,
- 2 m Temperature averaged for all grid points.

The best hyperparameters, based on the tuning performed as described in Section 2.3, are:

- 20–20 neurons in two hidden layers,
- a learning rate of 0.001,
- ReLU activation function.

The MLP with 355 inputs and 20–20 neurons organized into two hidden layers network has 7561 parameters, which is already sufficient to learn this complex relationship.

The five performance metrics are presented in Table 4 individually for the three years of 2019–2021 and also overall for the whole three-year period. The correlation coefficient is high, and the errors are relatively low in all years; therefore, the modeling can be deemed quite accurate. The MBE and variance ratio have some year-to-year variance, but overall they are close to 0 and 100%, respectively. In line with these metrics, the histogram in Fig. 1 (a) also demonstrates that the distribution of the modeled dataset fits well with the measured one. The time series plot in Fig. 1 (b) shows that the biggest errors are around the midday peaks, but the direction of the differences varies daily, which means that there is no systemic error in the estimations. In Fig. 2, the differences between the modeled and real values of the hourly resolution PV plant capacity factors are plotted as a heat map for the years 2019–2021. This representation allows to easily track if there was a systematic time-dependent error pattern in the modeled data. The analysis of the data in Fig. 2 shows no sign of systematic error in the modeled data as the direction of the deviations varies over the whole year.

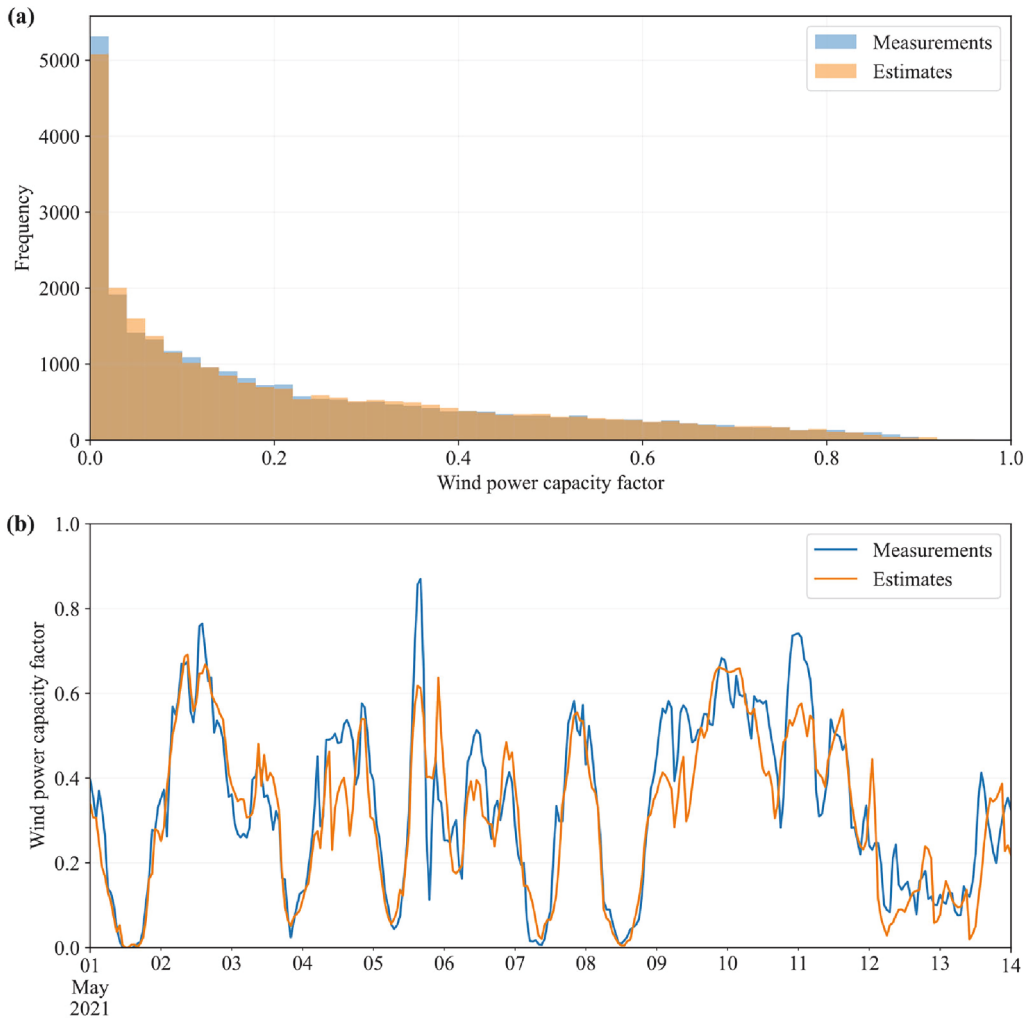

Fig. 3. Hourly national wind power capacity factor observations and estimates, (a) histogram for the three years of 2019–2021, (b) time series plot for a randomly selected sample period of 1st to 14th May 2021.

3.2. Wind power capacity factor modeling (WIND_ML model)

The most influential factor on wind turbine power production is the wind speed at the height of the turbine hubs. The typical hub height of MW-scale wind turbines is around 80–120 m; therefore, the 100 m wind speed is the most relevant predictor. Theoretically, it is possible to correct the wind speed for different heights by the power law [55], but as long as the exact heights of the wind turbines are not known in detail, no such correction is applied. The power of the wind turbine also depends on the density of air, which is influenced by the ambient temperature. The temperature at the hub height is slightly lower than at 2 m height, but the machine learning model is expected to account for this difference.

The power in the wind, which is proportional to the cube of the wind speed, and a theoretical wind turbine power output, calculated by applying a theoretical power curve on the wind speed data, were also tested as further predictors. However, in our experience, these predictors have slightly decreased the accuracy of the modeled data instead of improving it; therefore, they are not used in the final model.

The predictand of the MLP is the aggregated national wind power capacity factor, while the predictors are (532 inputs in total):

- *u* component of the 100 m wind speed individually for all grid points,
- *v* Component of the 100 m wind speed individually for all grid points,
- absolute value of the 100 m wind speed individually for all grid points,
- *2* m Temperature averaged for all grid points.

The best hyperparameters based on the performed tuning process are:

- 20–20 neurons in two hidden layers,
- a learning rate of 0.001,
- hyperbolic tangent activation function.

The performance metrics for the wind turbine capacity factors are presented in Table 5. The correlation coefficient is lower, the errors are higher, and the year-to-year variability is also higher for the wind power capacity factor compared to the PV capacity factor, which is in line with the results of other studies [31,32]. The average capacity factor of the wind power is also higher than that of the PV; therefore, compared to the mean value, the errors are not significantly higher. The reason for the relatively higher errors is the cubic dependence of the power on the wind speed, which highly exaggerates the wind speed errors of the reanalysis.

According to the histograms shown in Fig. 3 (a), the distributions of the measured and modeled data are very similar. The time series plot of Fig. 3 (b) shows that even though the model is not able to track all the rapid but smaller changes in the wind power, it can properly reproduce

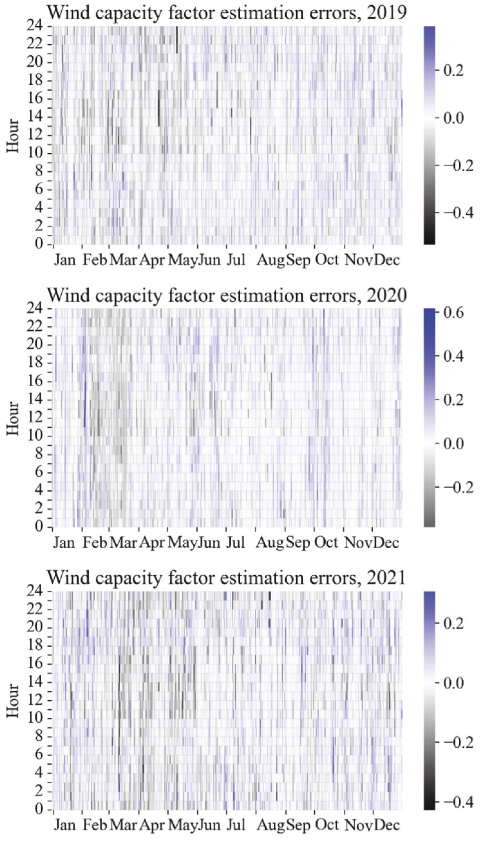

Fig. 4. Time-dependence of the hourly wind power capacity factor errors with WIND_ML model.

Table 5
Error metrics of the national wind power capacity factor estimations in WIND_ML model. All metrics are calculated for the cross-validation steps when the given year is used as the test data.

	2019	2020	2021	Overall
Correlation coefficient	0.947	0.935	0.945	0.942
MBE	0.002	0.004	0.001	0.002
MAE	0.054	0.055	0.050	0.053
RMSE	0.076	0.081	0.073	0.077
Variance ratio	90.1%	111.8%	94.8%	98.2%

the main tendencies and follow the bigger changes, and it captures 98.2% of the real variability of the wind power production. At this point, it is important to note that these favorable results are largely attributed to variance correction presented in Section 2.4. The error metrics and the distribution and time series plots of the raw, uncorrected modeled wind capacity factors are presented in Appendix B, along with a discussion on the main benefits of the proposed variance correction. The heat maps of the wind power capacity factor modeling errors in Fig. 4 show no time-dependent systematic errors. However, here with WIND_ML model the maximum errors are larger than for the PV power plants with the PV_ML model, which is in line with the error metrics reported in Table 4 and 5.

3.3. Electric load profile modeling (LOAD_ML model)

The electric load profile has a very characteristic time dependence, which can be described as the superposition of a typical daily, weekly and seasonal pattern. To model this, the day of the year, day of the week, and hour of the day are included among the predictors. The electricity demand on holidays also differs from the ordinary days, therefore, a binary variable specifying whether the given timestamp is on holiday or not is also added to the predictors.

Finally, the electric load is also affected by the weather, which is important to consider, as the main point of using historical weather data is to model how the given weather conditions affect the generation and load profiles [56]. For example, a general tendency is that in good weather conditions with high solar irradiance and low wind speed, people tend to spend more time outdoors, reducing domestic electricity demand. Fortunately, if the amount of training data is sufficient, the machine learning model can learn the connection between the meteorological variables and the load conditions without the need to dig deeper into the underlying effects and causes.

The predictand of the MLP is the mean-normalized electric load, The predictors of the MLP are (seven inputs in total):

- Ambient temperature averaged for all grid points
- Absolute wind speed averaged for all grid points
- Global horizontal irradiance averaged for all grid points
- Day of year
- Hour of day
- Day of week
- Holiday

The best hyperparameters based on the performed tuning process are:

- 200 neurons in a single hidden layer,
- a learning rate of 0.001,
- ReLU activation function.

The performance metrics are summarized in Table 6 individually for each year and averaged for all six years. Overall, the accuracy of the modeled data is between the wind and PV power capacity factor estimations. Comparing the different years, the errors are significantly higher in 2021 than in the other years, which can be attributed to the prolonged effect of the COVID-19 pandemic, and the increasing installed capacity of the behind-the-meter household-scale PV systems in Hungary.

The distribution of the modeled electric load, similarly to the PV and wind capacity factors, aligns well with the distribution of the measured data, as shown by the histograms in Fig. 5 (a). The time series plots are shown for the same period of two different years, 2017 and 2021, in Fig. 5 (b) and (c). In 2017, the modeled load profiles fit well with the measured load, but in 2021 the model overestimates the midday part of the profiles on most days. The difference between the estimated and measured load profiles resembles the PV capacity factors in Fig. 1 (b) (please note how the low PV production on 8th May aligns with the low

Table 6
Error metrics of the mean-normalized electric load estimations. All metrics are calculated for the cross-validation steps when the given year is used as the test data.

	2015	2016	2017	2018	2019	2021	Overall
Correlation coefficient	0.971	0.975	0.977	0.976	0.969	0.933	0.966
MBE	0.003	−0.003	0.000	−0.002	−0.006	0.002	−0.001
MAE	0.026	0.024	0.023	0.023	0.027	0.039	0.027
RMSE	0.034	0.031	0.030	0.031	0.035	0.051	0.036
Variance ratio	99.7%	98.1%	103.2%	102.0%	100.2%	95.6%	99.8%

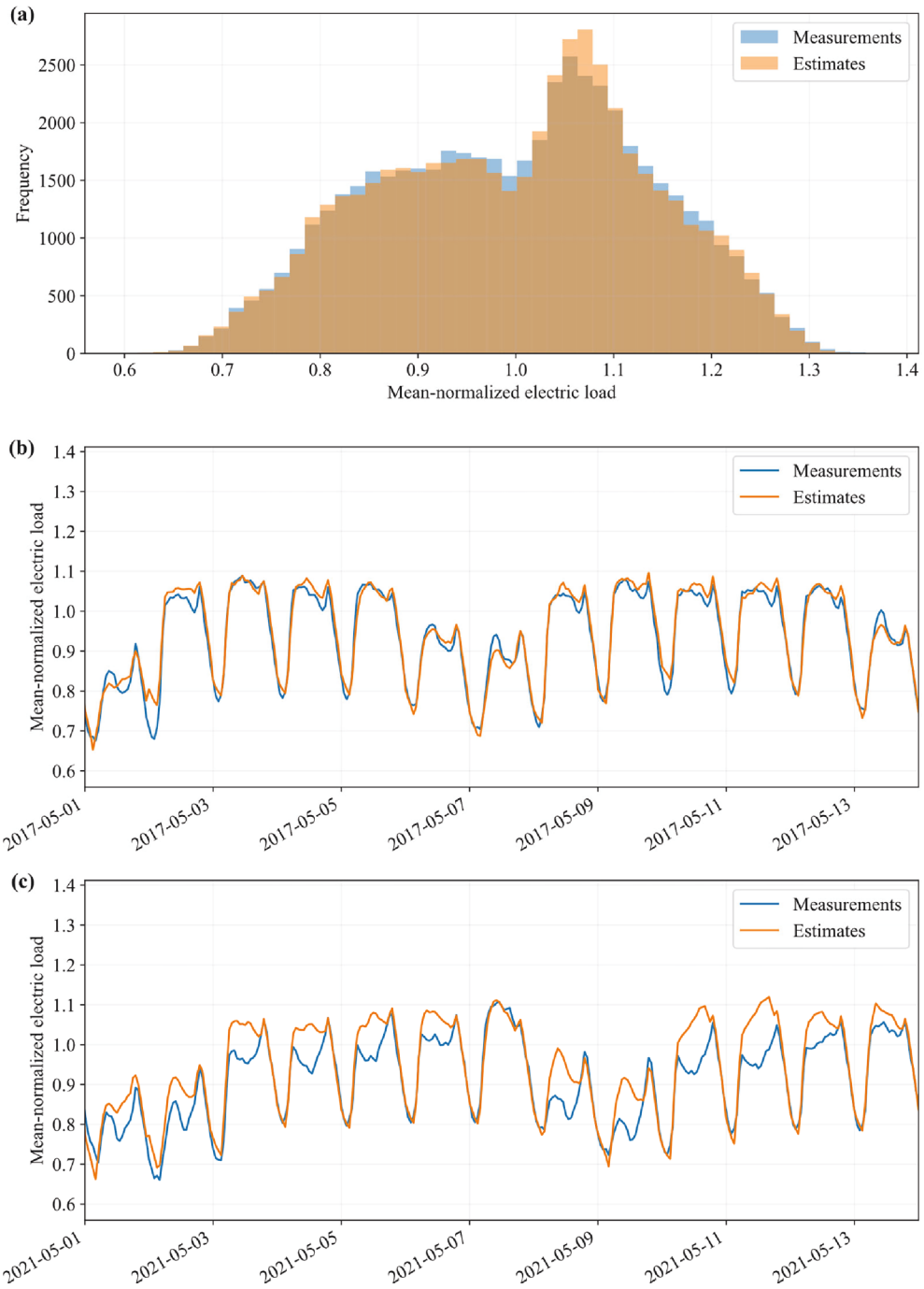

Fig. 5. Hourly mean-normalized electric load observations and estimates, (a) histogram for the six years of 2015–2019 and 2021, (b) and (c) time series plot for randomly selected sample periods of 1st to 14th May 2017 and 2021, respectively.

errors in the load estimation on the same day), which supports that the higher errors in 2021 are largely due to the behind-the-meter PV production. Due to technical reasons, the power output of the household-scale PV systems is not measured separately in Hungary, but it only appears in the reduction of the load on sunny days. The load reduction due to these PV systems could be accounted for by the LOAD_ML model based on the solar irradiance predictor. However, the installed capacity of these systems was significantly lower in the 2015–2019 period compared to 2021; therefore, this load reduction appeared to a much lower extent in training than in the test data (in the cross-validation, as described in the introduction of Section 3, the model used for making the estimations for 2021 is trained on the data of the other years).

Fig. 6 shows the heatmap of the errors of the load modeling for 2015–2021. The effect of household-scale PV systems can be clearly seen in these plots: in 2015–2018, when the installed capacity of the Hungarian household-scale PV systems was still low, the model slightly underestimates the load during daytime, whereas for 2021, there is a massive daytime overestimation of the system load. Aside from this effect, there is no so time-dependent systematic error that would span across all the years.

The lower accuracy for the year 2021 highlights the importance of the behind-the-meter renewable energy production on the load profile modeling. If the installed capacity of these household-scale renewable generators increases from year to year, and their production profile is not measured separately, they can deteriorate the accuracy of the load profile estimations. In this study, the installed capacity of the household-

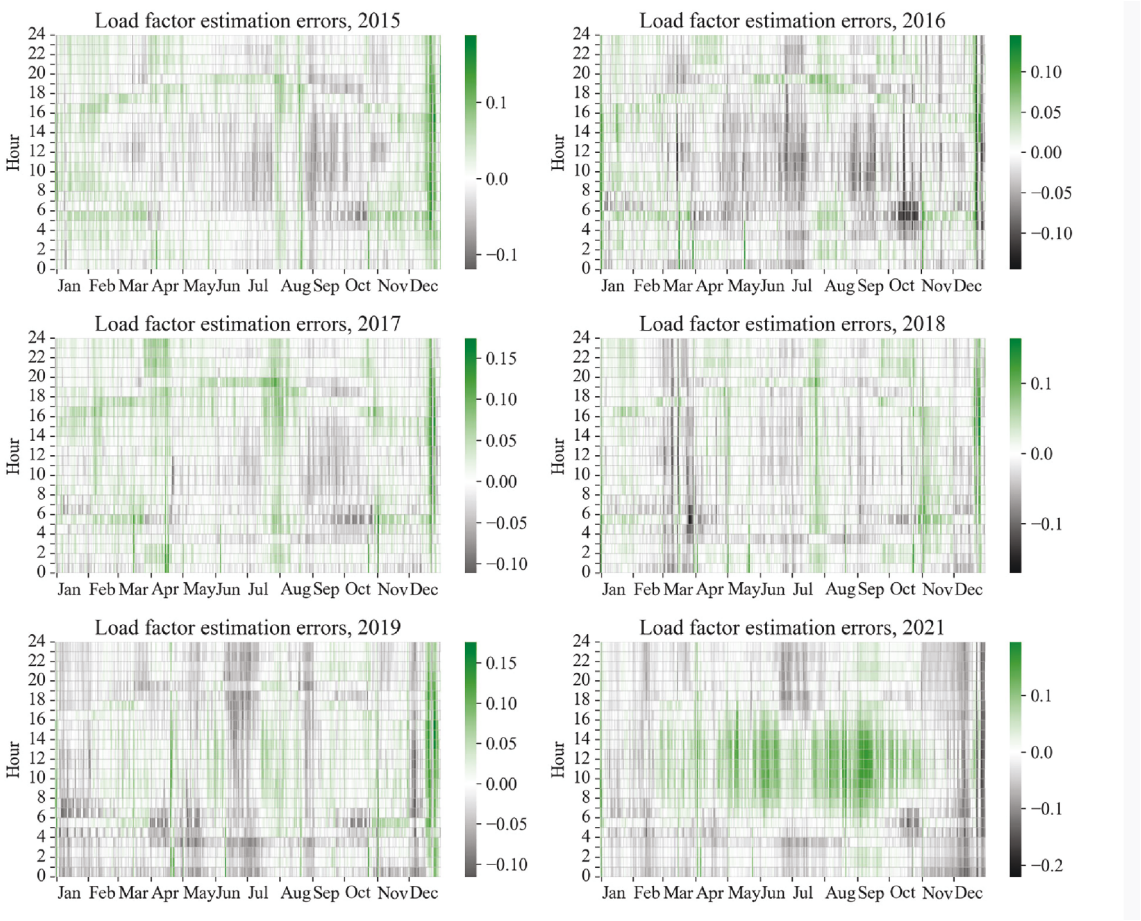

Fig. 6. Time-dependence of the hourly electric load estimation errors.

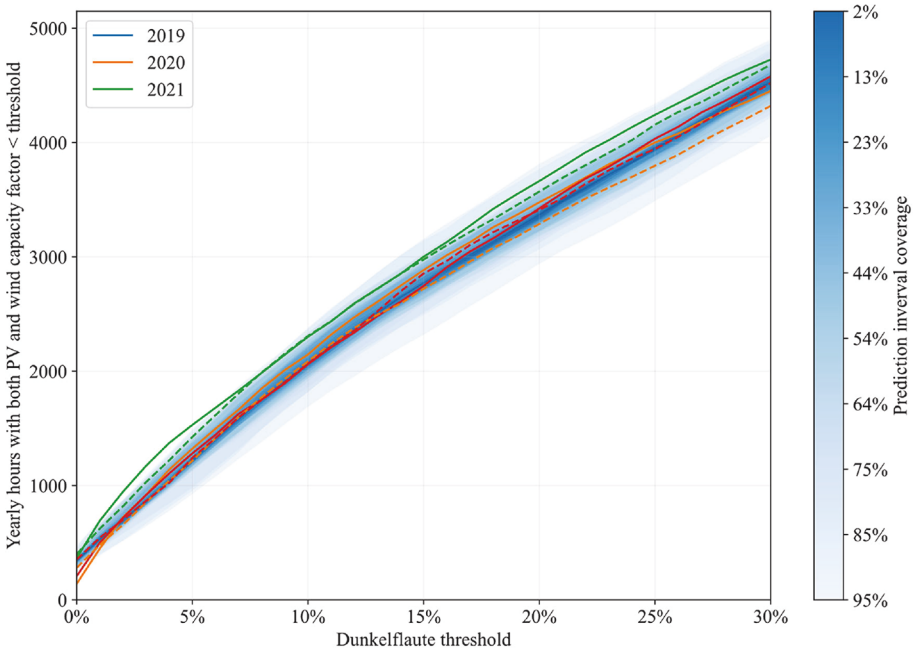

Fig. 7. Yearly number of Dunkelflaute hours for different thresholds with prediction intervals calculated from the 42 years of modeled data. Solid and dashed lines indicate the results calculated from the real and modeled data for 2019–2021, respectively.

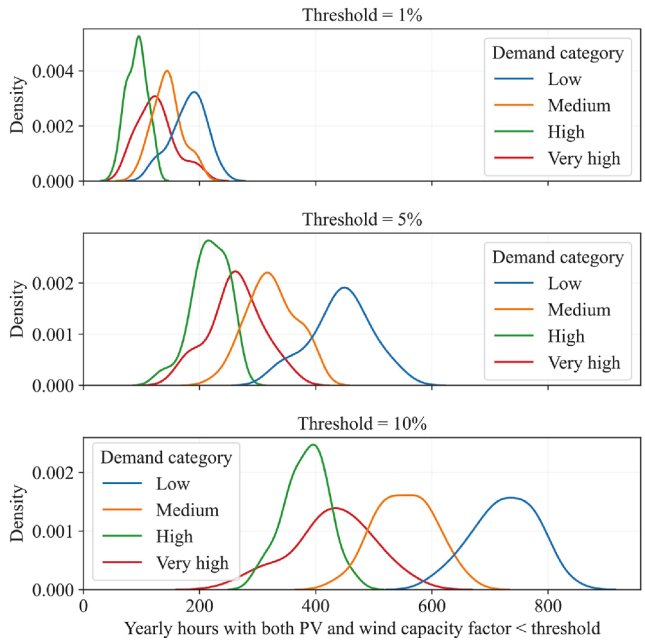

Fig. 8. Probability density function, calculated from the 42 yearly modeled data, of the yearly number of Dunkelflaute hours (PV and wind capacity factors are simultaneously below a threshold) for three different thresholds, grouped by demand categories.

scale PV systems is relatively low during most training years; therefore, it can be assumed that the modeled load profile shows the real load with only a low behind-the-meter PV production. As proposed for example in or [17] study, accurate measurement and central data collection of behind-the-meter PV production units by the TSO would be extremely important to reduce the above mentioned errors.

3.4. Limitations

As with all simulations, the presented method also relies on several assumptions that may pose limitations on the use of the modeled profiles. First, it is assumed that the weather will similarly develop in the future as it has in the past, and climate change has no decisive effect on renewable energy production or electricity consumption.

Second, it is assumed that the installed capacity of the PV and wind power plants will have the same geographical distribution over the country as today, and the design parameters of the new installations will also be the same as those of the existing plants. As we do not know how these factors will change in a long time horizon, this is a fair assumption, except for such cases where there are still so few renewable power plants that they are not distributed well enough and are not representative in the long run. However, if it can be known that further renewable energy projects will be developed in new locations or systematic changes in the design parameters can be expected, the presented ML-based method can be extended by physical modeling, in which the production of these atypical plants are modeled by wind power curves and PV model chains directly from the meteorological data.

Third, the load profile is assumed to be similar in the future as today. This means that the effects of further electrification and the demand changes due to the increasing penetration of electric cars and heat pumps are not taken into account. In such cases, the method presented here can be used to propagate the current profiles to the future, which can be freely supplemented with expected future trends even with several different scenarios if needed.

4. Possible applications and discussion

This section presents two possible applications of the hourly production and load profiles generated by the introduced machine learning method. One possible application is the modeling of Dunkelflaute events, which are the periods when the production of both solar PV and wind power plants are low. These events are worth investigating because they pose the highest risk to the security of the electricity supply in electricity systems with high solar and wind penetration. The other application is estimating the share of the electricity demand that renewable energy sources can cover, which metric is a common target of energy strategy documents. The following subsections demonstrate how the 42-years-long modeled profiles can be used to make probabilistic estimations that also quantify the year-to-year variability of the calculated metrics. The theoretical background behind these topics and the exact methods and equations used to derive the results presented herein are summarized in Section 2.5.

4.1. Dunkelflaute modeling

DF events can best be characterized by their annual frequency, which is shown in Fig. 7 as a function of the threshold value. The width of the prediction intervals, even with a 95% nominal coverage, is relatively small, with lower and upper bounds around ± 15% from the mean. To test the reliability of the results based on the data estimated by the ML model, individual curves are also plotted for the years 2019 to 2021; the solid lines show the results for the real (which are used for the training) and the dashed lines for the modeled (synthetic) capacity factor data. The number of DF hours is underestimated by the modeled data for most thresholds in all years, but the difference between the results for the real and modeled data is lower than the difference between the years. Therefore, even despite its slight underestimation, it is still more reliable to use multiple years of modeled data instead of the real data of one single arbitrary year, which justifies the usefulness of the proposed method.

The results in Fig. 7 show that in Hungary, the annual frequency of DF events never reaches zero, neither for the modeled nor for the real values, which means that around 200–400 h should be expected every year with absolutely no weather-dependent renewable energy production. The annual DF hours are between 950 and 1450 for 5% and 1700–2300 for 10% thresholds. These results also provide an opportunity to compare the Hungarian values with calculations for other countries. For the 10% threshold, the Belgian data show 600–700 DF hours per year [2], the EU28-wide DF can occur in 750–2000 h a year according to different data series [44], and the German system is expected to have 600 DF hours on a yearly basis if only wind power generation is considered [2]. According to these results, DF is more frequent in Hungary than in Belgium or Germany; therefore, Hungary should pay more attention to the prediction and proper management of these events. The high frequency of DF confirms that it is essential to have conventional power plants or appropriate grid-scale storage capacities in the future Hungarian electricity system to ensure the stable operation of the electricity system during these critical periods.

4.2. Dunkelflaute event classification

DF is calculated only from the capacity factor of both the PV and wind power plants; however, in practice, the negative consequences of the DF events largely depend on the electricity demand. The DF during the peak load hours poses a higher risk to the stability of the grid than a DF during low demand. Following this idea, it is possible to classify the DF hours into different demand categories. The demand category is assigned to each hour of the year depending on which quartile the load profile is in the given hour.

- Q1: DF event in very high demand period.

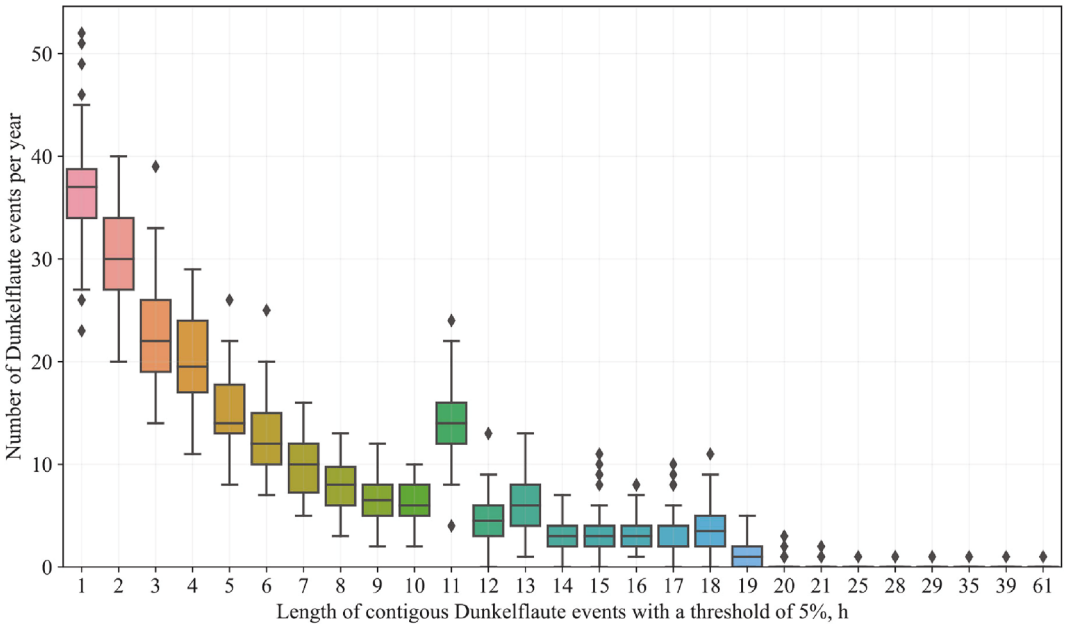

Fig. 9. Boxplots for the number of individual Dunkelflaute events grouped by length for a 5% threshold.

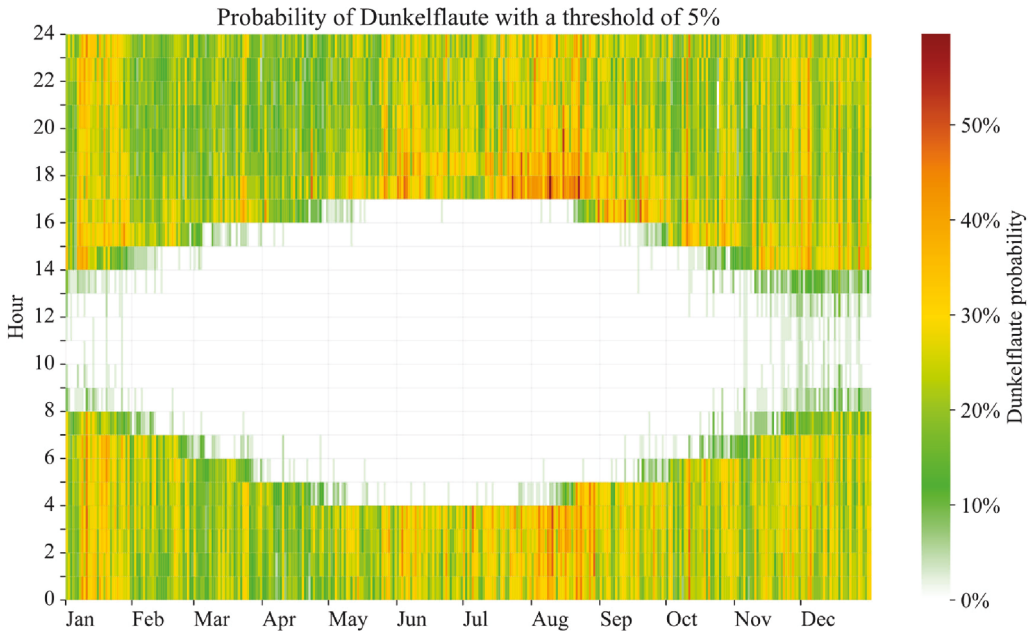

Fig. 10. Heatmap of the probability of DF hours with a 5% threshold for all hours of the year, calculated from the 42 years of modeled capacity factors.

- Q2: DF event in high demand period.
- Q3: DF event in medium demand period.
- Q4: DF event in low demand period.

The probability density functions of the number of DF hours in each category are shown in Fig. 8 for 1%, 5%, and 10% thresholds.

The definition of DF is that both wind and PV power has low capacity factors, which mostly occur during the night when the solar PV production reduces to zero. The nighttime typically covers the daily peak with the highest load several hours after sunset, but most of the night is associated with low electricity demand. This is in line with the results of Fig. 8, where most of the DF hours fall into the medium and low demand categories. However, the number of DF hours falling into the very high and high demand categories is also high, so the identification and analysis of these events are important for the security of supply of the electricity system.

The exact risk of a DF event could be assessed by a detailed model that includes the entire electricity system (consumption, renewable and conventional generation units, cross-border capacities, and electricity storage units). With such a model, one possible consequence of DF events, the amount of unserved electricity, could be quantified, which could be used as a basis for making clear statements about the future security of supply risk of the Hungarian electricity system. The construction of such a model is beyond the scope of the current paper but could be the topic of future research.

The severity of a DF event depends not only on the electricity demand but also on its duration. A DF ranging over only a few hours is easier to cover with energy storage compared to longer events. To

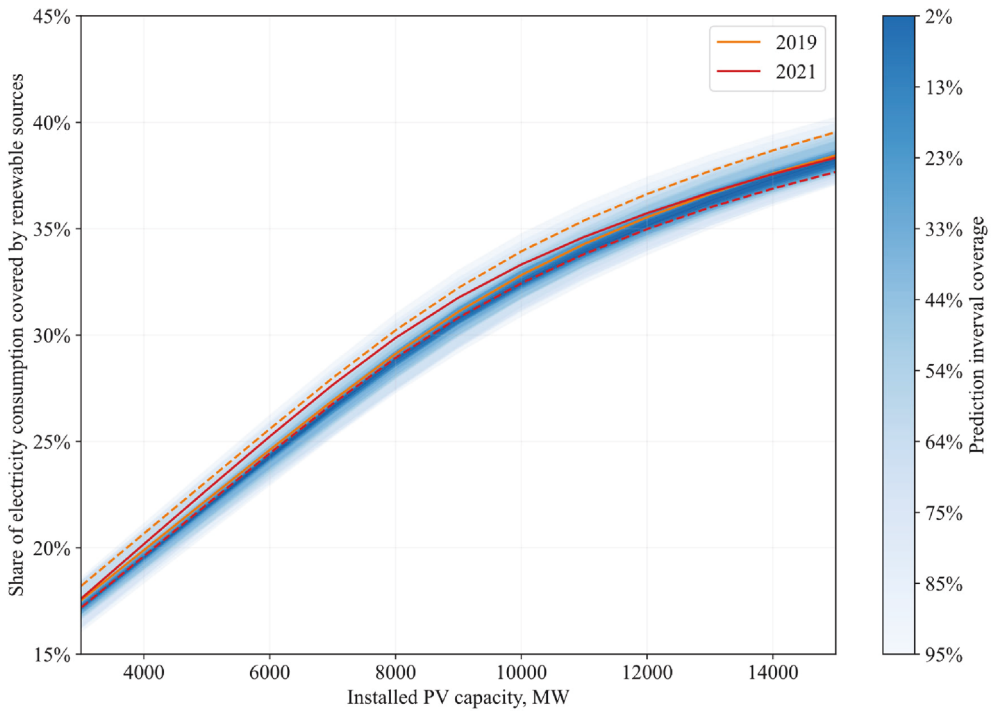

Fig. 11. Proportion of the electricity consumption that can be covered by PV and wind power generation in 2030 as function of solar PV capacities, assuming 3000 MW wind capacity. Solid and dashed lines indicate the results calculated from the real and modeled capacity factor and normalized load data, respectively.

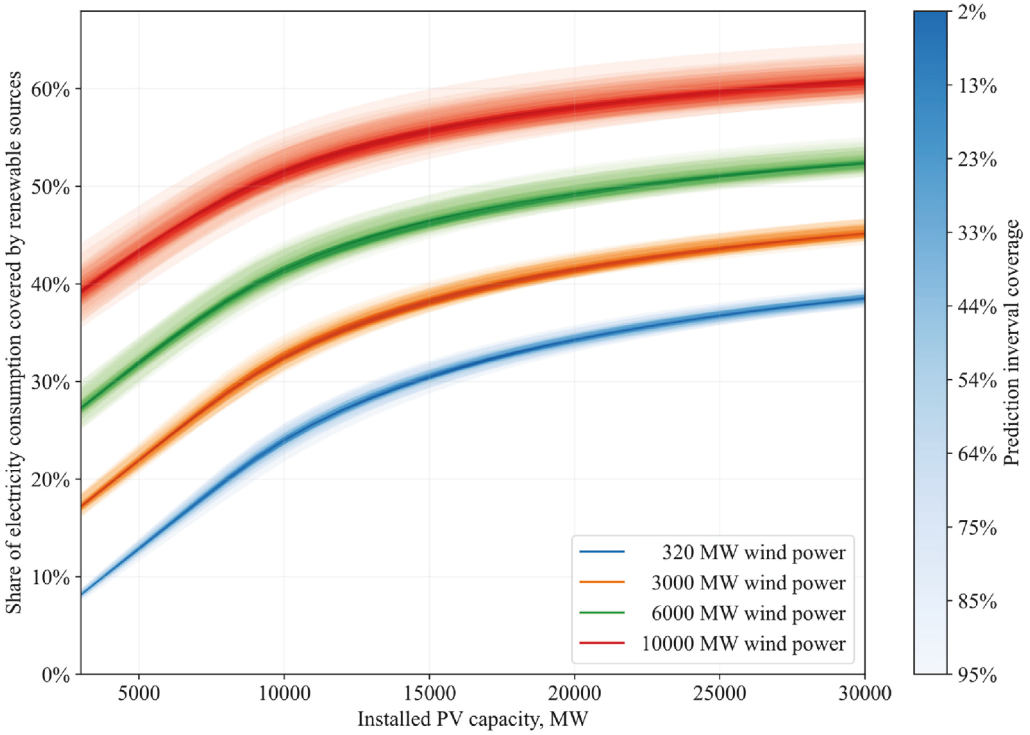

Fig. 12. Proportion of the electricity consumption that can be directly covered by PV and wind power generation in 2030.

analyze the expected duration of contiguous DF events, Fig. 9 presents the boxplots of the yearly number of DF events of different lengths evaluated for the 42 years for a 5% threshold. The boundaries of the box indicate the lower and upper quartiles, the line inside the box stands for the median, the whiskers show the rest of the distribution within 1.5 times of the interquartile range, while the dots represent the outliers.

4.3. Temporal distribution of Dunkelflaute hours

The frequency of DF events decreases as a function of length, with the exception of the 11-hour-long event frequency, for which a

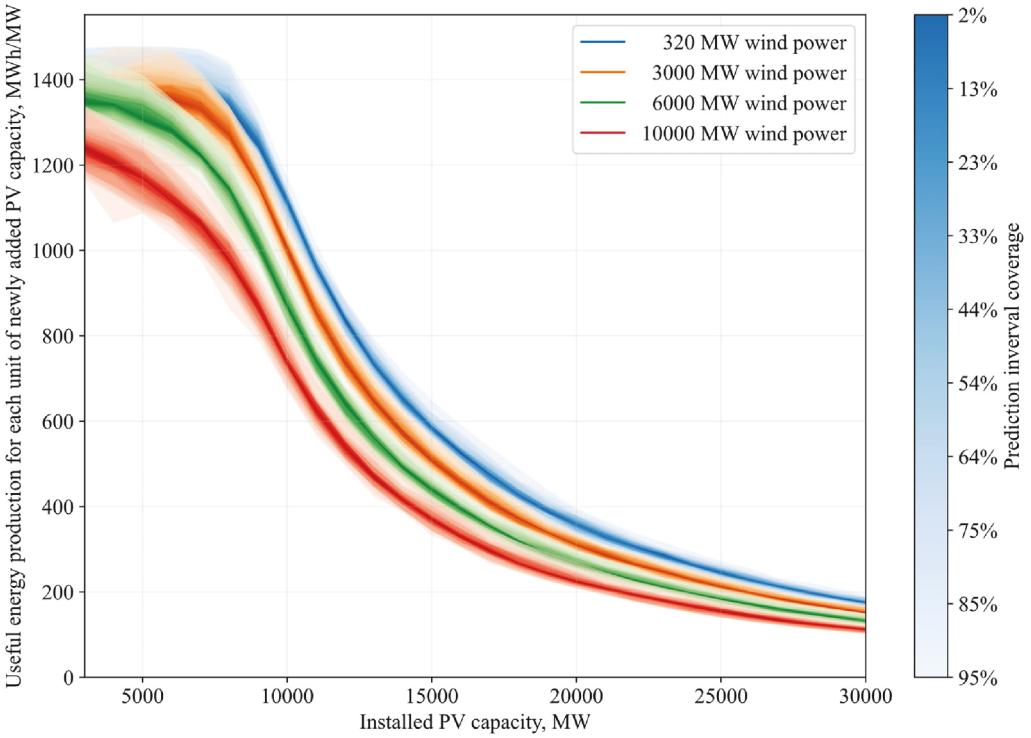

Fig. 13. Probabilistic diagrams of the useful specific energy production for each unit of newly added installed PV capacity in 2030 for different installed wind turbine capacities.

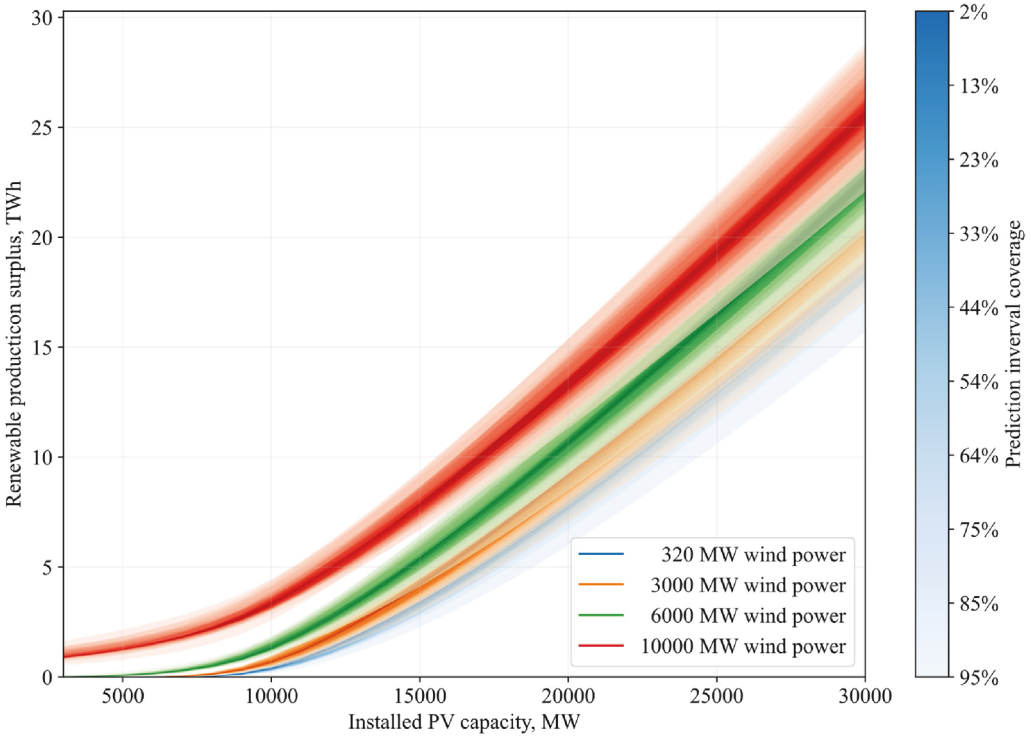

Fig. 14. Excess electricity of the PV and wind power generators above the coverage of the domestic electricity demand in 2030.

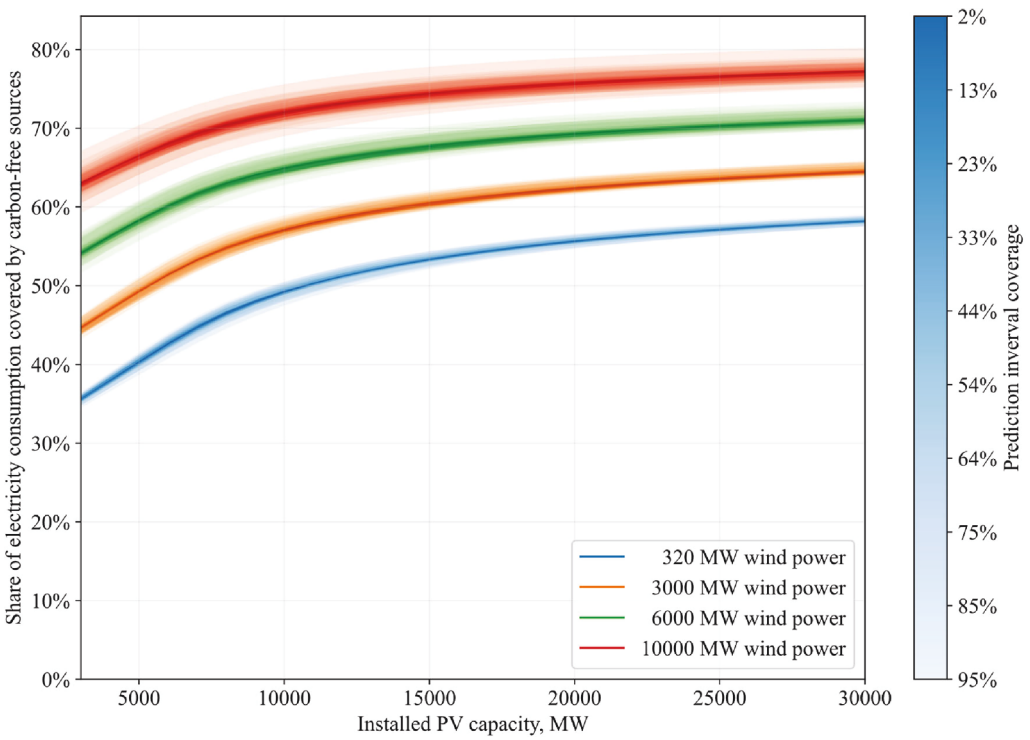

Fig. 15. Proportion of the electricity consumption that can be covered by carbon-free PV, wind, and nuclear (2000 MW installed capacity) power generation in 2030.

Table A7
Error metrics of the PV power capacity factor estimations for different installed PV capacity data resolutions and downscaling methods.

	Monthly data		Yearly data	
	Interpolated	Filled	Interpolated	Filled
Correlation coefficient	0.985	0.985	0.985	0.983
nMBE	0.000	0.004	−0.004	0.046
nMAE	0.021	0.021	0.021	0.050
nRMSE	0.042	0.043	0.042	0.096
Variance ratio	99.5%	103.6%	94.7%	162.3%

Table B8
Error metrics of the wind power capacity factor estimations without variance correction.

	2019	2020	2021	Overall
Correlation coefficient	0.947	0.935	0.945	0.941
nMBE	0.000	0.003	0.001	0.001
nMAE	0.056	0.054	0.051	0.054
nRMSE	0.078	0.078	0.072	0.076
Variance ratio	81.0%	103.1%	85.9%	89.3%

significant peak in the results emerges. This peak is due to the fact that DF events typically occur at night and the average length of these sunless periods is approximately 11 h in Hungary.[9] The maximum length that occurs on a yearly basis (i.e., the median is higher than zero) is 19 h, and the longest DF event in the 42 years of data lasts more than 2.5 days.

In addition to the annual frequency and duration of a DF event, it is important to analyze when the event occurs within the year. To determine this, the probability of whether an hour is DF or not is plotted on a heatmap in Fig. 10. Based on the analysis of Fig. 10 and the hourly value of the utilization factor of solar and wind power plants in Hungary presented in [17], it can be stated that DF events typically occur when there is no solar generation and are most frequent in the winter and August-September months when weather conditions are unfavorable for wind-based power generation. The overall highest probability of DF is in August in the hours before sunrise and after sunset. Daytime DF only occurs in winter, but they have a relatively low probability even during this period.

4.4. Possible role of renewable and nuclear energy in 2030

In this section, 42 years of data series computed with the ML models are fed into the simplified electricity supply model presented in Section 2.5. The electricity supply model applies to the electricity system of Hungary in 2030 (presented in the introduction and in sections 2.2 and 2.5). The average electricity system load is assumed to be 6602.6 MW based on government documents. All results are calculated for different values of installed PV and wind turbine capacities in order to analyze the effects of the increasing penetration of these renewable generation capacities.

Fig. 11 shows the share of electricity consumption that can be directly covered by domestic PV and wind power production as a function of installed PV capacity, assuming 3000 MW of installed wind turbine capacity. The shape of the curve is concave, which means that as PV capacity increases, the added value of new capacity decreases due to the fact that the increasing renewable power generation will eventually exceed the system demand, resulting in overproduction in the system. The relative width of the prediction intervals is only around ±5–10% from the mean, which is even smaller than for the DF hours presented in Fig. 7.

The results for 2019 and 2021 are shown with solid lines for the real and dashed lines for the ML-modeled capacity factor data. The real data, in this case, refers to the capacity factor and normalized load data derived from the TSO, which are, similarly to the modeled data, scaled for 2030 by the expected PV and wind capacities and total electricity demand. The use of the modeled data still leads to a small inaccuracy, but the direction of the errors is different for the two years, which

[9] https://www.worlddata.info/europe/hungary/sunset.php.

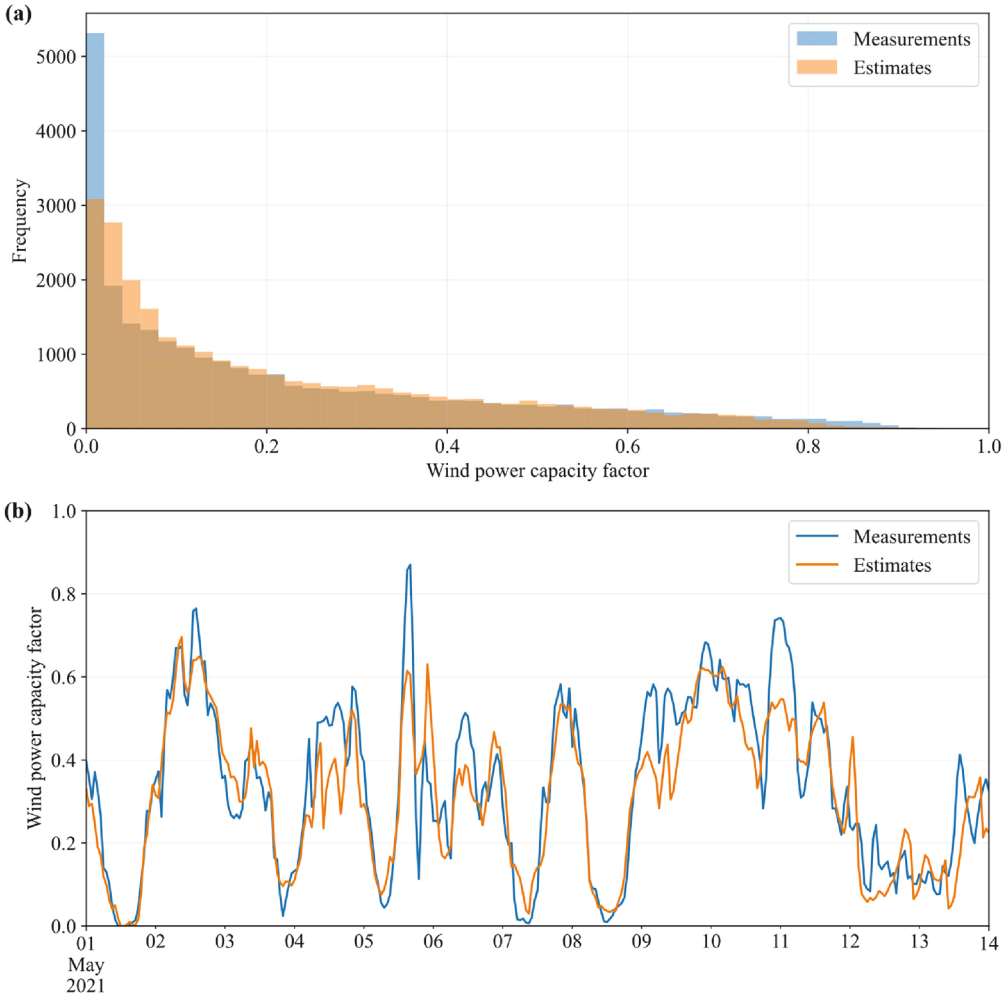

Fig. B16. Hourly wind power capacity factor observations and estimates without variance correction, (a) histogram for the three years of 2019–2021, (b) time series plot for a sample period of 1st to 14th May 2021.

suggests that there is no systematic overestimation or underestimation; therefore, the modeled results can be deemed quite reliable.

Fig. 12 is similar to Fig. 11, except that it plots the renewable share up to higher installed PV and four different installed wind turbine capacities. The percentages on the vertical axis can be easily converted to the annual amount of useful renewable power generation by multiplying them by 57.839 TWh, the assumed total annual electricity consumption in the year 2030.

Analyzing the data in Fig. 12, the following statements can be made:

- Without energy storage, the recommended capacity of PV power plants is around 10–12 GW. Above this point, the added value of further PV capacity additions largely decreases; thus, it is better to invest in wind turbines or in other type of production capacities.
- The year-to-year variance of the estimated renewable share (represented by the width of the prediction intervals) increases significantly with increasing installed wind power capacity, while it is only slightly affected by the PV capacity. This means that the probabilistic modeling method proposed in this paper is even more important in countries with high wind power capacity than in countries with high PV capacity.
- Even for the maximum examined renewable capacity, which is around five times the peak load of the Hungarian system, the renewable share is still only around 60%, which is far from the 100% renewable goals. This result shows that the 100% decarbonization of electricity production cannot be achieved only by increasing the installed renewable generating capacities, but other carbon-free electricity generation units and/or grid scale electricity storage is also essential.

Fig. 13 shows the derivative of the useful energy production by the installed PV power; in other words, the useful annual energy production of each MW of newly installed PV power plants. The added value (i.e., the directly useable electricity production) of the new PV installations starts to decrease rapidly right from 5 to 6 GW installed PV power, and it is only around half of its total energy production at only 10 GW installed PV.

The amount of excess energy produced by the wind turbines and PV plants is shown in Fig. 14. Depending on the conditions, this energy must either be exported, stored, or curtailed. Overproduction arises at the earliest when there is 5–8 GW of installed solar capacity (except when there are 10 GW of wind capacity in the system), which means that when the installed capacity of solar power plants in the Hungarian system reaches this level, the Hungarian TSO and the policy makers should have a plan in place for what to do with this unused electricity. The export of unused electricity from the overproduction of solar power plants is also questionable, because if the neighboring countries increase the installed capacity of solar power plants according to their planned energy strategy [17], there will be no market for this electricity in the region and only storage or curtailment will be a real option to solve the problem, if

Table C9
Summary of previous research on modeling electricity demand and renewable production profiles using different methods and databases.

Authors	Year of publication	Timestep	Meteorological data	Estimation of profiles	Method	Evaluation of the generated data series (GDS)	Use of the GDS	Domain
Matsuo et al. [58]	2020	hourly	AMeDAS	- Solar: from solar irradiance data (empirical) - Wind: from wind velocity (power law) - Demand: artificial neural network	Linear Programming, Cummulative Residual Load	- Solar: nothing - Wind: nothing Demand: Comparison of the estimated and actual electric demands (R2 = 0.9678)	Analysis of: Power storage requirement - Substitution among the VRE technologies Substitution between storage systems - The role of firm capacities	Japan
Ohba et al. [4]	2022	hourly	AMeDAS	Solar and wind generation reconstructed by observational data (wind velocity, surface air temperature and sunshine duration)	Self-Organizing Map	- Solar: Comparison of the estimated and actual electric demands (R2 = 0.987814) Wind: Comparison of the estimated and actual electric demands (R2 = 0.992623) - correlation coefficient in learning period greater than 0.98 while outside of the learning period is about 0.94	- Investigation of dark doldrum events for a period of one (DD1), three (DD3), or five (DD5) days - SOM to establish a link between various WPs and their impact on local VRE	Thoku region (Japan)
Li et al. [2]	2020	quarter-hourly	Belgium specific datasets	–	Weather Research and Forecasting	–	Recreating a Dunkelflaute event with the WRF model and comparing the results of the model with observational data (wind speed, wind direction, wind power, shortwave radiation, temperature, sensible heat flux)	near the coast of Belgium
Guo et al. [59]	2018	–	Weather-related factors (rainfall levels, daily temperatures, etc.)	Load forecasting with RF, GBM and DL methods	Multi-layer Perceptron	The performance of a model is evaluated by the MRPE, MAPE, and MAE	- load foresting purposes (deep neural network) - investigate the performance of a deep neural network with (MLP) functions - identifying the most influential factors - data visualizations explore electricity consumption patterns	Three case studies in China
Bedi and Toshniwal [60]	2019	quarter-hourly	–	Load forecasting with four regression models - SVM, ANN, RNN and LSTM	Deep learning based framework	- Assessing the prediction accuracy of the learning/ regression models with RMSE, R and MAPE - R2 are between 0.653 and 0.96 for typical days	Predicting the electricity demand of UT Chandigarh with SVM, ANN, RNN and LSTM	India
Ohlendorf and Schill [3]	2020	hourly	MERRA-2 dataset	Wind generation from wind velocity (logarithmic power law) at three types of wind zones (based on mean local wind speeds)	Aggregating capacity factors of wind power plants using a weighting scheme considering the current distribution of wind power in Germany	–	- Analyze two different (MBT and CBT) LWP periods of 2%, 5% and 10% capacity factor - Seasonal distribution and frequency of LWP events - Magnitude of the most extreme LWP	Germany

(*continued on next page*)

Table C9 (*continued*)

Authors	Year of publication	Timestep	Meteorological data	Estimation of profiles	Method	Evaluation of the generated data series (GDS)	Use of the GDS	Domain
							events - Spatial distribution of wind power during most extreme LWP event	
Huang et al. [61]	2020	hourly	Temperature and humidity (there are also non-meteorological input data such as historical load, electricity price and the type of the day)	Load range discretization method to generate LPD for CNN	Convolutional Neural Network	The comparisons of load probabilistic forecasting results based on 7 methods	- Generating load probability distributions - Optimizing the load probability distributions for training samples	New England
Huang et al. [62]	2020	hourly	Solar irradiance, temperature humidity and historical photovoltaic power	Daily-ahead probabilistic PV power forecasting method based on an improved QCNN	quantile Convolutional Neural Network	Five metrics to evaluate the prediction effect, including RMSE, MAPE, SCC, PICP and PINAW.	- Analysis of the predicted PV powers with different quantiles - Comprehensive analysis of the prediction results of the different methods - Demonstration of the daily-ahead probabilistic PV power forecasting result based on QCNN - Prediction effect of QCNN under different weather conditions	–
Livas-García et al. [19]	2022	hourly	SMN-CLICOM / IEM	Demand: ANN	ANN, Global Sensitive Analysis, Multi-layer Perceptron	Demand: R2 = 0.9104 – 0.9241	Electricity market forecast	Mexican southeast region
Sharifzadeh et al. [18]	2019	hourly	Renewables.ninja website	- Solar: solar power, temperature, direct and diffuse irradiance - Wind: wind power, temperature and wind speed at 10 m - Demand: electricity energy - Hourly and seasonal variables were used in all 3	ANN, Support Vector Regression, Gaussian Process Regression	- MPE: solar 10.38%, wind: 8.3% and demand: 3.67% - R2: solar: nothing, wind: R2 after 6-step: 0.94 (ANN) and demand: nothing	Predicting wind and solar production and electricity demand	- Solar and wind: Canterbury, UK - Demand: 1 157 households
Dosdogru et al. [63]	2022	hourly and daily	Winnipeg Weatherstats.	- Wind: predicting wind speed based on hybrid methods (XGBoost, ANN, AdaBoost) and determining parameter optimizing with PSO	Extreme Gradient Boosting, Adaptive Boosting, ANN, PSO	- Taylor diagram (SD, RMSD, R) - The performance of a models is evaluated by RMSE, MSE, MAE and CPU	Wind speed prediction	Winnipeg
Mensour et al. [64]	2017	daily and monthly	Souss-Massa specific meteorological data	Solar: average monthly solar radiation using ANN based on geographical and meteorological data	ANN, Multi-layer Perceptron	- The performance is validated by RMSE, MAE and R - Measured and predicted values correlation coefficient R = 0.98725	Predicting global monthly solar radiation	South-West of Morocco
Elattar et al. [65]	2020	hourly	Other publications	Probabilistic approach based on (2 m + 1) point estimate method and ESSA to model the uncertainties in solar generation, wind generation, load demand and market prices	Efficient Salp Swarm Algorithm, Slap Swarm Algorithm	Evaluated using a typical grid-connected microgrid.	Predicting solar generation, wind generation, load demand and market prices	–

there will be enough storage capacities that time (this is not the case at the moment). The scale of the problem could be decreased in the future by relying on synergies of sector coupling (eg. electricity, transport, heating, electrification of heavy industry) [57]. Moreover, the real amount of excess energy will be even higher than the modeled values due to the part-load operation constraints and the limited load change rate of conventional power plants.

Fig. 15 is similar to Fig. 12, with the difference that it shows the share of not only renewable but the whole carbon-free electricity generation, which also includes the production of the 2000 MW nuclear power plant in Hungary. The significantly larger values in Fig. 15 than in Fig. 12 show that nuclear power is essential to achieve a high share of carbon-free electricity production. However, even with the existing nuclear power plant and very high PV and wind capacities, it is still not possible to reach the 90% carbon-free electricity generation target for 2030. This result shows that if Hungary is to meet its carbon-free electricity generation targets, it will need to invest in technologies that can either produce electricity in a similarly carbon-free way (nuclear, biomass, geothermal) or store electricity on a large scale and over a long time horizon (pumped storage, batteries, power-to-gas), in addition to solar and wind power plants.

This brief analysis does not account for energy storage. Without storage, even with the heavy overcapacities of renewable sources, it is hard to increase the share of renewable electricity above 40–50%. Installing energy storage will also increase the added values of the further PV and wind capacities, as it can reduce curtailment by storing the excess energy. Import and export options are also not considered, but it should be noted that exporting is a viable way of using excess energy, but its availability depends on the neighboring countries and the available cross-border transmission capacities.

A simplification of the above-presented electricity supply model is that the maximum ramp-up and ramp-down rates and the minimum part-load power of conventional power plants are not considered. These constraints reduce the useful power and thus increase the excess energy production of PV and wind power plants in reality compared to the model, which means that the share of renewables in the real electricity system will be even lower than presented above. More accurate results could only be achieved by creating a detailed electricity market model, which is out of the scope of the present study, but an important direction for future research.

5. Conclusions

In this study, an easy-to-use neural network model is proposed to link weather factors to the solar and wind power generation and electric load and to create hourly-resolution synthetic profiles based on 42 years of atmospheric reanalysis weather data. To reduce statistical errors between synthetic and real data, a variance-correction technique is also presented in this article. The profiles for multiple decades enable performing probabilistic analyses that can quantify the uncertainty resulting from the year-to-year variability of weather in the simulations. The proposed method is demonstrated for Hungary in this paper, but it can be implemented to any country where sufficient data on renewable energy production and electricity consumption are available.

Two applications of the proposed method are presented through the example of Hungary, namely the investigation of Dunkelflaute (DF) events and the analysis of renewable and carbon neutral electricity generation through a simplified electricity supply model. The results show that with a 10% threshold, the number of DF hours is 1800–2300 in Hungary, higher than in the countries studied in the literature (Belgium, Germany). Therefore, Hungary should invest sufficient resources in dealing with these events, e.g., installing conventional power plants and/or sufficient electricity storage capacities, to ensure the continuous supply. To evaluate the severity of DF events, a novel categorization method based on electricity consumption was introduced. The majority of DF hours fall into the low (Q1) or medium (Q2) consumption category, but the number of hours in the high (Q3) and very high (Q4) categories is also high, which highlights the need for a more accurate analysis of these events. Most of the DF events last only for a few hours, but longer-term events of up to 19 h can be expected on an annual basis, too.

The results of the Hungarian electricity supply model for 2030 show that even with a very high installed renewable capacity of 30 GW photovoltaic (PV) and 10 GW wind power, the direct renewable generation can only cover up to 60% of the annual consumption. If the nuclear power plant in Hungary is also considered, it is possible to reach a much higher carbon-free share in the electricity consumption even with lower renewable generating capacities, which underlines the role of nuclear power in meeting the emission reduction targets. The uncertainty of the renewable share modeling is more affected by the installed wind turbine capacity than by the PV capacity. The directly usable electricity production of new PV plants starts to decrease significantly above 5–6 GW of installed capacity, which calls for the investment in large electricity storage capacities to make use these capacities instead of curtailing their overproduction. The model results also indicate that energy policy decisions need to be supported by high – at least hourly – resolution simulations, as opposed to the current practice, which is to rely on annual balances and simulations of representative days.

Possible future works include the extension of the presented machine learning model to other countries and the development of an electricity market model that includes different countries, individual power plants, storage facilities, and cross-border capacities in order to better understand the probability of DF events and the associated security of supply risks at both the Hungarian and the European electricity system level.

CRediT authorship contribution statement

Martin János Mayer: Conceptualization, Methodology, Software, Validation, Formal analysis, Data curation, Visualization, Writing – original draft. **Bence Biró:** Conceptualization, Investigation, Validation, Data curation, Visualization, Writing – original draft. **Botond Szücs:** Investigation, Validation, Writing – original draft. **Attila Aszódi:** Conceptualization, Investigation, Validation, Writing – review & editing, Supervision.

Declaration of Competing Interest

The authors declare that they have no known competing financial interests or personal relationships that could have appeared to influence the work reported in this paper.

Data availability

The data used in this paper is freely available, and it is described in the text how the interested readers can obtain it.

Acknowledgment

The research reported in this paper is part of project no. BME-NVA-02, implemented with the support provided by the Ministry of Innovation and Technology of Hungary from the National Research, Development and Innovation Fund, financed under the TKP2021 funding scheme. This paper was also supported by the National Research, Development and Innovation Fund, project no. OTKA-FK 142702 and ÚNKP-22-5-BME-305, and the János Bolyai Research Scholarship of the Hungarian Academy of Sciences.

Appendix

Appendix A. . Effect of the availability of PV installed capacity data

The renewable power production is available with an hourly resolution from most data sources; however, the installed capacity is typically only published with a monthly or even yearly resolution (e.g., the ENSTO-E Transparency Platform contains only a single installed capacity value for each year). To calculate the hourly capacity factor, the installed capacity data must be downscaled to hourly resolution, which can be done either by interpolating or filling. Filling means that all hourly values of the given month or year are considered the same as the single available data, while interpolation assumes a linear increase of the installed capacity over time between the known data points.

In Hungary, the installed capacity of wind turbines was constant over the studied three-year period, while the installed utility-scale PV capacity increased from 423 MW at the beginning of 2019 to 1829 MW at the end of 2021. To examine the effect of the different downscaling strategies and the resolution of the installed capacity data, the errors of the PV capacity factor modeling, calculated in the same way as in Section 3.1, are shown in Table A7. Overall, the best accuracy belongs to the case when monthly data are interpolated, so this should be the recommended practice if the data availability allows it. However, the results calculated for the interpolated yearly data are almost the same as for the monthly data, which means that the presented method can also be used without any significant error increase, even if the installed capacity is only available on a yearly basis. The downscaling by filling is generally not recommended, especially for yearly data, as it largely increases the modeling errors.

Appendix B. . Effect of the variance correction on the wind power estimates

This appendix presents the evaluation of the raw wind power capacity factor outputs of the ML model without the variance correction presented in Section 2.4. As a comparison, the variance-corrected results are described in Section 3.2. The error metrics of the raw estimations are summarized in Table B8. The average variance ratio for the three years is only 89.3% for the uncorrected estimations, which clearly shows their underdispersion, while the variance ratio of the corrected estimations is significantly higher, 98.2%. Otherwise, the error metrics are not significantly affected by the variance correction.

The histograms in Fig. B16 (a) also indicate the underdispersion of the raw estimations, as there are significantly fewer extremely low and higher capacity factor values in the modeled dataset than in the measured. The tendency that the raw estimations vary in a narrower range than the real measured capacity factors is also apparent in Fig. B16 (b). In the one hand, the lack of extremely low values can cause a significant error in the modeling of the DF events, as the number of DF hours is, by definition, directly connected to the frequency of the low capacity factor values. On the other hand, the lack of extremely high values underestimates the overproduction of renewable energy sources and thus the resulting curtailment, and overestimates the share of the electricity consumption that can be covered by renewables. Consequently, such severely underdispersed datasets are practically unusable for these applications. Fortunately, as shown in Fig. B16 in Section 3.2, the variance correction can effectively reduce the underdispersion and make the modeled capacity factor time series suitable for the reliable modeling of the DF events and the future energy mix. See Fig. B16 and Table B8.

Appendix C. . Comparative table of key literature references

See Table C9.

References

[1] Hille E, Althammer W, Diederich H. Environmental regulation and innovation in renewable energy technologies: Does the policy instrument matter? Technol Forecast Soc Change 2020;153:119921. https://doi.org/10.1016/J.TECHFORE.2020.119921.

[2] Li B, Basu S, Watson SJ, Russchenberg HWJ. Mesoscale modeling of a "Dunkelflaute" event. Wind Energy 2021;24:5–23. https://doi.org/10.1002/WE.2554.

[3] Ohlendorf N, Schill WP. Frequency and duration of low-wind-power events in Germany. Environ Res Lett 2020;15:084045. https://doi.org/10.1088/1748-9326/AB91E9.

[4] Ohba M, Kanno Y, Nohara D. Climatology of dark doldrums in Japan. Renew Sustain Energy Rev 2022;155:111927. https://doi.org/10.1016/J.RSER.2021.111927.

[5] Rokhmawati A. Comparison of power plant portfolios under the no energy mix target and national energy mix target using the mean–variance model. Energy Rep 2021;7:4850–61. https://doi.org/10.1016/J.EGYR.2021.07.137.

[6] Hori K, Kim J, Kawase R, Kimura M, Matsui T, Machimura T. Local energy system design support using a renewable energy mix multi-objective optimization model and a co-creative optimization process. Renew Energy 2020;156:1278–91. https://doi.org/10.1016/J.RENENE.2019.11.089.

[7] Shirizadeh B, Quirion P. Do multi-sector energy system optimization models need hourly temporal resolution? A case study with an investment and dispatch model applied to France. Appl Energy 2022;305:117951. https://doi.org/10.1016/J.APENERGY.2021.117951.

[8] Liu Y, Zhang J, Zhu Z, Zhao G. Impacts of the 3E (economy, energy and environment) coordinated development on energy mix in China: The multi-objective optimisation perspective. Struct Chang Econ Dyn 2019;50:56–64. https://doi.org/10.1016/J.STRUECO.2019.05.005.

[9] Casalicchio V, Manzolini G, Prina MG, Moser D. From investment optimization to fair benefit distribution in renewable energy community modelling. Appl Energy 2022;310:118447. https://doi.org/10.1016/J.APENERGY.2021.118447.

[10] Singh P, Meena NK, Yang J, Vega-Fuentes E, Bishnoi SK. Multi-criteria decision making monarch butterfly optimization for optimal distributed energy resources mix in distribution networks. Appl Energy 2020;278:115723. https://doi.org/10.1016/J.APENERGY.2020.115723.

[11] Weijermars R, Taylor P, Bahn O, Das SR, Wei YM. Review of models and actors in energy mix optimization – can leader visions and decisions align with optimum model strategies for our future energy systems? Energ Strat Rev 2012;1:5–18. https://doi.org/10.1016/J.ESR.2011.10.001.

[12] Kim D, Hur J. Short-term probabilistic forecasting of wind energy resources using the enhanced ensemble method. Energy 2018;157:211–26. https://doi.org/10.1016/J.ENERGY.2018.05.157.

[13] Schulz B, el Ayari M, Lerch S, Baran S. Post-processing numerical weather prediction ensembles for probabilistic solar irradiance forecasting. Sol Energy 2021;220:1016–31. https://doi.org/10.1016/J.SOLENER.2021.03.023.

[14] Mashlakov A, Kuronen T, Lensu L, Kaarna A, Honkapuro S. Assessing the performance of deep learning models for multivariate probabilistic energy forecasting. Appl Energy 2021;285:116405. https://doi.org/10.1016/J.APENERGY.2020.116405.

[15] Kim SO, Hur J. Probabilistic power output model of wind generating resources for network congestion management. Renew Energy 2021;179:1719–26. https://doi.org/10.1016/J.RENENE.2021.08.014.

[16] Dumas J, Wehenkel A, Lanaspeze D, Cornélusse B, Sutera A. A deep generative model for probabilistic energy forecasting in power systems: normalizing flows. Appl Energy 2022;305:117871. https://doi.org/10.1016/J.APENERGY.2021.117871.

[17] Aszódi A, Biró B, Adorján L, Dobos ÁC, Illés G, Tóth NK, et al. Comparative analysis of national energy strategies of 19 European countries in light of the green deal's objectives. Energy Conversion and Management: X 2021;12:100136. https://doi.org/10.1016/J.ECMX.2021.100136.

[18] Sharifzadeh M, Sikinioti-Lock A, Shah N. Machine-learning methods for integrated renewable power generation: A comparative study of artificial neural networks, support vector regression, and Gaussian Process Regression. Renew Sustain Energy Rev 2019;108:513–38. https://doi.org/10.1016/J.RSER.2019.03.040.

[19] Livas-García A, May Tzuc O, Cruz May E, Tariq R, Jimenez Torres M, Bassam A. Forecasting of locational marginal price components with artificial intelligence and sensitivity analysis: A study under tropical weather and renewable power for the Mexican Southeast. Electr Pow Syst Res 2022;206:107793. https://doi.org/10.1016/J.EPSR.2022.107793.

[20] Pöstges A, Bucksteeg M, Ruhnau O, Böttger D, Haller M, Künle E, et al. Phasing out coal: An impact analysis comparing five large-scale electricity market models. Appl Energy 2022;319:119215. https://doi.org/10.1016/J.APENERGY.2022.119215.

[21] Abrell J, Eser P, Garrison JB, Savelsberg J, Weigt H. Integrating economic and engineering models for future electricity market evaluation: A Swiss case study. Energ Strat Rev 2019;25:86–106. https://doi.org/10.1016/J.ESR.2019.04.003.

[22] Arriagada E, López E, López M, Blasco-Gimenez R, Roa C, Poloujadoff M. A probabilistic economic dispatch model and methodology considering renewable energy, demand and generator uncertainties. Electr Pow Syst Res 2015;121:325–32. https://doi.org/10.1016/J.EPSR.2014.11.018.

[23] Rakipour D, Barati H. Probabilistic optimization in operation of energy hub with participation of renewable energy resources and demand response. Energy 2019;173:384–99. https://doi.org/10.1016/J.ENERGY.2019.02.021.

[24] Li L, Ling L, Yang Y, Poursoleiman R. Modeling and optimal energy operation considering probabilistic and sustainable renewable energy models and demand

side management. Energy Build 2021;231:110557. https://doi.org/10.1016/J.ENBUILD.2020.110557.
[25] Coelho CAS, Cardoso DHF, Firpo MAF. Precipitation diagnostics of an exceptionally dry event in São Paulo. Brazil Theor Appl Climatol 2016;125:769–84. https://doi.org/10.1007/S00704-015-1540-9/FIGURES/10.
[26] Empinotti VL, Budds J, Aversa M. Governance and water security: The role of the water institutional framework in the 2013–15 water crisis in São Paulo. Brazil Geoforum 2019;98:46–54. https://doi.org/10.1016/J.GEOFORUM.2018.09.022.
[27] Marengo Orsini JA, Alves LM, Alvala RCS, Cunha AP, Brito S, Moraes OLL. Climatic characteristics of the 2010–2016 drought in the semiarid Northeast Brazil region. An Acad Bras Cienc 2017;90:1973–85. https://doi.org/10.1590/0001-3765201720170206.
[28] Ostojic G, Stankovski S, Ratkovic Z, Miladinovic L, Maksimovic R. Development of hydro potential in Republic Srpska. Renew Sustain Energy Rev 2013;28:196–203. https://doi.org/10.1016/J.RSER.2013.07.036.
[29] Wohland J, Eddine Omrani N, Keenlyside N, Witthaut D. Significant multidecadal variability in German wind energy generation. Wind Energy Science 2019;4:515–26. https://doi.org/10.5194/WES-4-515-2019.
[30] Baumgartner J, Gruber K, Simoes SG, Saint-Drenan YM, Schmidt J. Less Information, Similar Performance: Comparing Machine Learning-Based Time Series of Wind Power Generation to Renewables.ninja. Energies 2020, Vol 13, Page 2277 2020;13:2277. Doi: 10.3390/EN13092277.
[31] Staffell I, Pfenninger S. Using bias-corrected reanalysis to simulate current and future wind power output. Energy 2016;114:1224–39. https://doi.org/10.1016/J.ENERGY.2016.08.068.
[32] Pfenninger S, Staffell I. Long-term patterns of European PV output using 30 years of validated hourly reanalysis and satellite data. Energy 2016;114:1251–65. https://doi.org/10.1016/J.ENERGY.2016.08.060.
[33] Ministry for Innovation and Technology. National Energy and Climate Plan. 2020.
[34] Ministry for Innovation and Technology. National Clean Development Strategy 2020-2050. 2019.
[35] Hersbach H, Bell B, Berrisford P, Hirahara S, Horányi A, Muñoz-Sabater J, et al. The ERA5 global reanalysis. Q J R Meteorolog Soc 2020;146:1999–2049. https://doi.org/10.1002/qj.3803.
[36] Gelaro R, McCarty W, Suárez MJ, Todling R, Molod A, Takacs L, et al. The Modern-Era Retrospective Analysis for Research and Applications, Version 2 (MERRA-2). J Clim 2017;30:5419–54. https://doi.org/10.1175/JCLI-D-16-0758.1.
[37] Yang D, Bright JM. Worldwide validation of 8 satellite-derived and reanalysis solar radiation products: A preliminary evaluation and overall metrics for hourly data over 27 years. Sol Energy 2020;210:3–19. https://doi.org/10.1016/j.solener.2020.04.016.
[38] Aszódi A, Biró B. A koronavírus járvány hatása a villamosenergia-rendszerre mint kritikus infrastruktúrára. Scientia et Securitas 2021;2:136–45. https://doi.org/10.1556/112.2021.00044.
[39] Markovics D, Mayer MJ. Comparison of machine learning methods for photovoltaic power forecasting based on numerical weather prediction. Renew Sustain Energy Rev 2022;161:112364. https://doi.org/10.1016/j.rser.2022.112364.
[40] Wang S, Takyi-Aninakwa P, Jin S, Yu C, Fernandez C, Stroe DI. An improved feedforward-long short-term memory modeling method for the whole-life-cycle state of charge prediction of lithium-ion batteries considering current-voltage-temperature variation. Energy 2022;254:124224. https://doi.org/10.1016/J.ENERGY.2022.124224.
[41] Voyant C, Notton G, Kalogirou S, Nivet ML, Paoli C, Motte F, et al. Machine learning methods for solar radiation forecasting: A review. Renew Energy 2017;105:569–82. https://doi.org/10.1016/j.renene.2016.12.095.
[42] Mayer MJ. Benefits of physical and machine learning hybridization for photovoltaic power forecasting. Renew Sustain Energy Rev 2022;168:112772. https://doi.org/10.1016/j.rser.2022.112772.
[43] Mayer MJ, Yang D. Calibration of deterministic NWP forecasts and its impact on verification. Int J Forecast 2022:In Press. Doi: Doi: 10.1016/j.ijforecast.2022.03.008.
[44] Kies A, Schyska BU, Bilousova M, el Sayed O, Jurasz J, Stoecker H. Critical review of renewable generation datasets and their implications for European power system models. Renew Sustain Energy Rev 2021;152:111614. https://doi.org/10.1016/J.RSER.2021.111614.
[45] Hirth L, Steckel JC. The role of capital costs in decarbonizing the electricity sector. Environ Res Lett 2016;11:114010. https://doi.org/10.1088/1748-9326/11/11/114010.
[46] Sepulveda NA, Jenkins JD, de Sisternes FJ, Lester RK. The Role of Firm Low-Carbon Electricity Resources in Deep Decarbonization of Power Generation. Joule 2018;2:2403–20. https://doi.org/10.1016/J.JOULE.2018.08.006.
[47] Murphy AH. The Coefficients of Correlation and Determination as Measures of performance in Forecast Verification. Weather Forecast 1995;10:681–8. https://doi.org/10.1175/1520-0434(1995)010<0681:TCOCAD>2.0.CO;2.
[48] Mayer MJ, Gróf G. Extensive comparison of physical models for photovoltaic power forecasting. Appl Energy 2021;283:116239. https://doi.org/10.1016/j.apenergy.2020.116239.
[49] Yang D. Solar radiation on inclined surfaces: Corrections and benchmarks. Sol Energy 2016;136:288–302. https://doi.org/10.1016/j.solener.2016.06.062.
[50] Bright JM, Engerer NA. Engerer2: Global re-parameterisation, update, and validation of an irradiance separation model at different temporal resolutions. J Renew Sustain Energy 2019;11:18. https://doi.org/10.1063/1.5097014.
[51] Perez R, Ineichen P, Seals R, Michalsky J, Stewart R. Modeling daylight availability and irradiance components from direct and global irradiance. Sol Energy 1990;44:271–89. https://doi.org/10.1016/0038-092X(90)90055-H.
[52] Gueymard CA, Ruiz-Arias JA. Extensive worldwide validation and climate sensitivity analysis of direct irradiance predictions from 1-min global irradiance. Sol Energy 2016;128:1–30. https://doi.org/10.1016/j.solener.2015.10.010.
[53] Reda I, Andreas A. Solar position algorithm for solar radiation applications. Sol Energy 2004;76:577–89. https://doi.org/10.1016/j.solener.2003.12.003.
[54] Mayer MJ, Gróf G. Techno-economic optimization of grid-connected, ground-mounted photovoltaic power plants by genetic algorithm based on a comprehensive mathematical model. Sol Energy 2020;202:210–26. https://doi.org/10.1016/j.solener.2020.03.109.
[55] Kikumoto H, Ooka R, Sugawara H, Lim J. Observational study of power-law approximation of wind profiles within an urban boundary layer for various wind conditions. J Wind Eng Ind Aerodyn 2017;164:13–21. https://doi.org/10.1016/J.JWEIA.2017.02.003.
[56] Behm C, Nolting L, Praktiknjo A. How to model European electricity load profiles using artificial neural networks. Appl Energy 2020;277:115564. https://doi.org/10.1016/J.APENERGY.2020.115564.
[57] Brown T, Schlachtberger D, Kies A, Schramm S, Greiner M. Synergies of sector coupling and transmission reinforcement in a cost-optimised, highly renewable European energy system. Energy 2018;160:720–39. https://doi.org/10.1016/J.ENERGY.2018.06.222.
[58] Matsuo Y, Endo S, Nagatomi Y, Shibata Y, Komiyama R, Fujii Y. Investigating the economics of the power sector under high penetration of variable renewable energies. Appl Energy 2020;267:113956. https://doi.org/10.1016/J.APENERGY.2019.113956.
[59] Guo Z, Zhou K, Zhang X, Yang S. A deep learning model for short-term power load and probability density forecasting. Energy 2018;160:1186–200. https://doi.org/10.1016/J.ENERGY.2018.07.090.
[60] Bedi J, Toshniwal D. Deep learning framework to forecast electricity demand. Appl Energy 2019;238:1312–26. https://doi.org/10.1016/J.APENERGY.2019.01.113.
[61] Huang Q, Wei S. Improved quantile convolutional neural network with two-stage training for daily-ahead probabilistic forecasting of photovoltaic power. Energy Convers Manag 2020;220:113085. https://doi.org/10.1016/J.ENCONMAN.2020.113085.
[62] Huang Q, Li J, Zhu M. An improved convolutional neural network with load range discretization for probabilistic load forecasting. Energy 2020;203:117902. https://doi.org/10.1016/J.ENERGY.2020.117902.
[63] Dosdoğru AT, Boru İA. Hybrid boosting algorithms and artificial neural network for wind speed prediction. Int J Hydrogen Energy 2022;47:1449–60. https://doi.org/10.1016/J.IJHYDENE.2021.10.154.
[64] Mensour ON, El Ghazzani B, Hlimi B, Ihlal A. Modeling of solar energy potential in Souss-Massa area-Morocco, using intelligence Artificial Neural Networks (ANNs). Energy Procedia 2017;139:778–84. https://doi.org/10.1016/J.EGYPRO.2017.11.287.
[65] Elattar EE, ElSayed SK. Probabilistic energy management with emission of renewable micro-grids including storage devices based on efficient salp swarm algorithm. Renew Energy 2020;153:23–35. https://doi.org/10.1016/J.RENENE.2020.01.144.